Coordination Chemistry Reviews 253 (2009) 779–794

Contents lists available at ScienceDirect

Coordination Chemistry Reviews

journal homepage: www.elsevier.com/locate/ccr

Review

Spectroscopically validated density functional theory studies of the B_{12} cofactors and their interactions with enzyme active sites

Thomas C. Brunold*, Karen S. Conrad, Matthew D. Liptak, Kiyoung Park

Department of Chemistry, University of Wisconsin-Madison, 1101 University Avenue, Madison, WI 53706-1322, USA

Contents

ARTICLE INFO

Article history:
Received 5 May 2008
Accepted 23 September 2008
Available online 17 October 2008

Keywords:
B_{12}-dependent enzymes
Density functional theory
Electronic structure description
Vitamin B_{12}

ABSTRACT

Vitamin B_{12} and its biologically active derivatives, 5′-deoxyadenosylcobalamin (AdoCbl) and methylcobalamin (MeCbl), have long fascinated chemists with their elaborate structures and unusual reactivities in enzymatic systems. Due to their large size and complex electronic structures, these cofactors have posed a major challenge for computational chemists. Yet, recent insights gained from kinetic, spectroscopic, and X-ray crystallographic studies, have established an excellent foundation for the successful completion of density functional theory studies aimed at elucidating the electronic structures of the isolated cofactors and the catalytic cycles of B_{12}-dependent enzymes. This review summarizes important information obtained from experimentally validated computational studies of: (i) the free AdoCbl and MeCbl cofactors in their Co^{3+}, Co^{2+}, and Co^{1+} oxidation states; (ii) the mechanism by which enzymes involved in the biosynthesis of AdoCbl accomplish the thermodynamically challenging $Co^{2+} \rightarrow Co^{1+}$ reduction; (iii) the strategies employed by AdoCbl-dependent enzymes to achieve a trillion-fold rate acceleration for the homolytic cleavage of the cofactor's Co—C(Ado) bond; and (iv) the means by which MeCbl-dependent methyltransferases accelerate the rate of methyl transfer via heterolytic Co—C(Me) bond cleavage by as much as six orders of magnitude and reactivate the accidentally oxidized form of the cofactor.

Abbreviations: Abs, electronic absorption; ACS, acetyl-coenzyme A synthase; Ado, adenosyl; AdoCbl, adenosylcobalamin; ATP, adenosine 5′-triphosphate; ATR, adenosyltransferase; B3LYP, Becke's three-parameter hybrid functional for exchange combined with the Lee–Yang–Par correlation functional; Cbl, cobalamin; CD, circular dichroism; CFeSP, corrinoid/iron-sulfur protein; CH_3THF, methyltetrahydrofolate; CNCbl, cyanocobalamin; Co^{3+}Cbl, cob(III)alamin; Co^{2+}Cbl, cob(II)alamin; Co^{1+}Cbl, cob(I)alamin; CP-SCF, coupled-perturbed self-consistent field; CT, charge transfer; DFT, density functional theory; DMB, 5,6-dimethylbenzimidazole; EPR, electron paramagnetic resonance; GM, glutamate mutase; hATR, human adenosyltransferase; Hcy, homocysteine; H_2OCbl^+, aquacobalamin; HOMO, highest occupied molecular orbital; IR, infrared; LA, long-axis; LDA, local density approximation; LF, ligand field; LUMO, lowest unoccupied molecular orbital; MCD, magnetic circular dichroism; Met, methionine; MetH, methionine synthase; $MeCbi^+$, methylcobinamide; MeCbl, methylcobalamin; MLCT, metal-to-ligand charge transfer; MMCM, methylmalonyl-CoA mutase; MMCoA, methylmalonyl-CoA; MO, molecular orbital; PBE, Perdew–Becke–Ernzerhof; PW-LDA, Perdew–Wang local density approximation; rR, resonance Raman; SA, short-axis; SCF, self-consistent field; SCoA, succinyl-CoA; TDDFT, time-dependent density functional theory; UV, ultraviolet; VWN5-LDA, Vosko–Wilk–Nusair-5 local density approximation; XAS, X-ray absorption spectroscopy.

* Corresponding author. Tel.: +1 608 265 9056.
E-mail address: brunold@chem.wisc.edu (T.C. Brunold).

0010-8545/$ – see front matter © 2008 Elsevier B.V. All rights reserved.
doi:10.1016/j.ccr.2008.09.013

1. Introduction

Vitamin B_{12}, otherwise known as cyanocobalamin (CNCbl), has been the subject of intense research ever since its isolation from the liver in 1948 [1], and particularly after the determination of its structure by X-ray crystallography in 1955 [2]. CNCbl is a member of the large family of cob(III)alamin (Co^{3+}Cbl) species, all of which contain a low-spin, six-coordinate Co^{3+} ion that is equatorially ligated by four nitrogen atoms from a tetrapyrrole macrocycle, termed the corrin ring (Fig. 1). This Co^{3+} center is axially coordinated by the intramolecular 5,6-dimethylbenzimidazole (DMB) base on the α ("lower") face and a variable group on the β ("upper") face, from which each form of Co^{3+}Cbl derives its name. The biologically active Co^{3+}Cbl species are adenosylcobalamin (AdoCbl) and methylcobalamin (MeCbl) [3], in which the β-axial position is occupied by an adenosyl (Ado) moiety and a methyl (Me) group, respectively. Homolytic cleavage of the Co—C bond of AdoCbl (e.g., via photolysis) or the one-electron reduction of any Co^{3+}Cbl by a chemical reducing agent produces the cob(II)alamin (Co^{2+}Cbl) state [4]. The change in oxidation state from Co^{3+} to Co^{2+} is accompanied by a reduction in the Co coordination number from six to five due to the loss of the variable β-ligand. Alternatively, heterolytic cleavage of the Co—C bond of MeCbl or the one-electron reduction of Co^{2+}Cbl generates cob(I)alamin (Co^{1+}Cbl), which contains a four-coordinate, square-planar Co^{1+} center that is solely ligated by the corrin macrocycle. At low pH and in certain enzyme active sites, the DMB moiety that normally serves as the lower axial ligand to the Co ion in the +3 and +2 oxidation states of the cofactor is displaced by a water molecule. A useful model for these DMB-off forms of the cofactor is provided by cobinamides, which are natural precursors of the cobalamin (Cbl) species that lack the nucleotide loop and DMB moiety and instead possess an axially bound water molecule in the Co^{3+} and Co^{2+} oxidation states (corresponding to Co^{3+}Cbi$^+$ and Co^{2+}Cbi$^+$, respectively).

Due to their large size and complex electronic structures, the quantum mechanical treatment of the Cbl cofactors represents a significant challenge for theoretical chemists. In recent years, density functional theory (DFT) has proven to be a particularly useful method for computational studies of Cbl systems. DFT appears to represent an ideal compromise in terms of accuracy and computational cost to meet the demands posed by the intricate Co electronic structure and the size of the corrin π-system. As a transition metal, the Co center requires an explicit treatment of the electronic structure and at least an approximate handling of electron correlation to yield an accurate theoretical description [5]. As a large π-system, the corrin ring contains too many electrons to treat electron correlation with a multi-configurational self-consistent field (SCF) approach [6–8]. DFT balances these demands of the Co center and the corrin macrocycle in a single reference configuration by explicitly treating the electronic structure and approximating electron correlation [9,10]. However, because of the approximations inherent to this approach, it is essential that the results obtained from DFT computations on Cbl species be validated on the basis of experimental data, such as X-ray crystal structures and spectroscopic parameters.

X-ray crystallography has been employed extensively to characterize a large number of Cbl species [11,12], and the three-dimensional structures obtained in these studies are excellently suited to assess the feasibility of DFT-optimized cofactor models. Additionally, a large library of spectroscopic data exists for vitamin B_{12} and many of its derivatives, providing an excellent framework for a thorough evaluation of the results obtained from DFT computations on these species. For example, DFT frequency calculations can be performed on geometry-optimized cofactor models to predict the compositions and frequencies of the normal modes of vibration. The results obtained in these calculations can be compared to the experimental frequencies of the corrin-based and, in the case of alkyl-Cbls, the Co—C stretching modes determined by resonance Raman (rR) spectroscopy [13–28]. Excited-state spectroscopic techniques such as electronic absorption (Abs), circular dichroism (CD), and magnetic CD (MCD) have proven to be excellent probes of Cbl electronic structures for all three Co oxidation states [26–28]. A combined analysis of the Abs, CD, and MCD spectra of a given Cbl species can be carried out to determine the energies and Abs intensities of individual electronic transitions, and this information can be used as the basis to evaluate the results obtained from time-dependent DFT (TDDFT) computations. Additionally, in the case of the paramagnetic forms Co^{2+}Cbl and Co^{2+}Cbi$^+$, electron paramagnetic resonance (EPR) spectroscopy offers an extremely sensitive probe of the axial bonding interactions and the unpaired spin density distribution. Consequently, a comparison between the experimental and DFT-computed **g** and **A** tensors provides an excellent means for validating calculated electronic structure descriptions [29–32]. Examples of how all of these spectroscopic techniques have been used to evaluate DFT computational results are provided in Section 2.

DFT computations have also been utilized with great success to interpret spectral changes accompanying the binding of Cbl species to enzyme active sites in terms of perturbations to the cofactors' geometric and electronic structures. In humans, the AdoCbl derivative of vitamin B_{12} is essential for the function of methylmalonyl-CoA mutase (MMCM), an enzyme that catalyzes the radical rearrangement of methylmalonyl-CoA (MMCoA) to succinyl-CoA (SCoA). This conversion is an important step in the catabolism of branched-chain amino acids, odd-chain fatty acids, and cholesterol [33–35]. In addition to MMCM, several other AdoCbl-dependent isomerases are known to exist in bacterial populations [36–40]. The biosynthesis of the AdoCbl cofactor required by these isomerases involves an intriguing Co—C bond formation step that is catalyzed by the ATP:corrinoid adenosyltransferase (ATR) enzymes, via the transfer of the Ado group from adenosine-5′-triphosphate (ATP) to a Co^{1+}Cbl intermediate [41–45]. The other biologically active form of vitamin B_{12}, MeCbl, is also used by a single enzyme in humans; namely, methionine synthase (MetH). MetH catalyzes the formation of methionine (Met) by transferring a methyl group from methyltetrahydrofolate (CH_3THF) to homocysteine (Hcy) [46,47]. This reaction is essential for maintaining a healthy distribution of cellular folate derivatives and preventing an accumulation of Hcy. Several additional Cbl-dependent methyltransferases are found in acetogens and methanogens [48,49]. The insights that DFT computations have provided into the catalytic cycles of enzymes involved in the biosynthesis of AdoCbl and of members of the two distinct classes of Cbl-dependent enzymes described above are discussed in Section 3.

2. The free cofactor

2.1. Co^{3+}corrinoids

Of the three accessible Co oxidation states of the free cofactor, the Co^{3+}Cbl state has been the subject of the majority of DFT studies reported to date [26,50–61]. In this state the central Co^{3+} ion is in a six-coordinate ligand environment, coordinated equatorially by the four nitrogens of the corrin macrocycle and axially ligated by a nitrogen from the tethered DMB base in the α-position and a variable ligand in the β-position. Although MeCbl and AdoCbl are the only enzymatically competent forms of the cofactor, DFT and TDDFT investigations have also been carried out on Co^{3+}Cbl species possessing other ligands in the β-axial position, such as CN (CNCbl or vitamin B_{12}) and H_2O (aquacobalamin, H_2OCbl$^+$) [26].

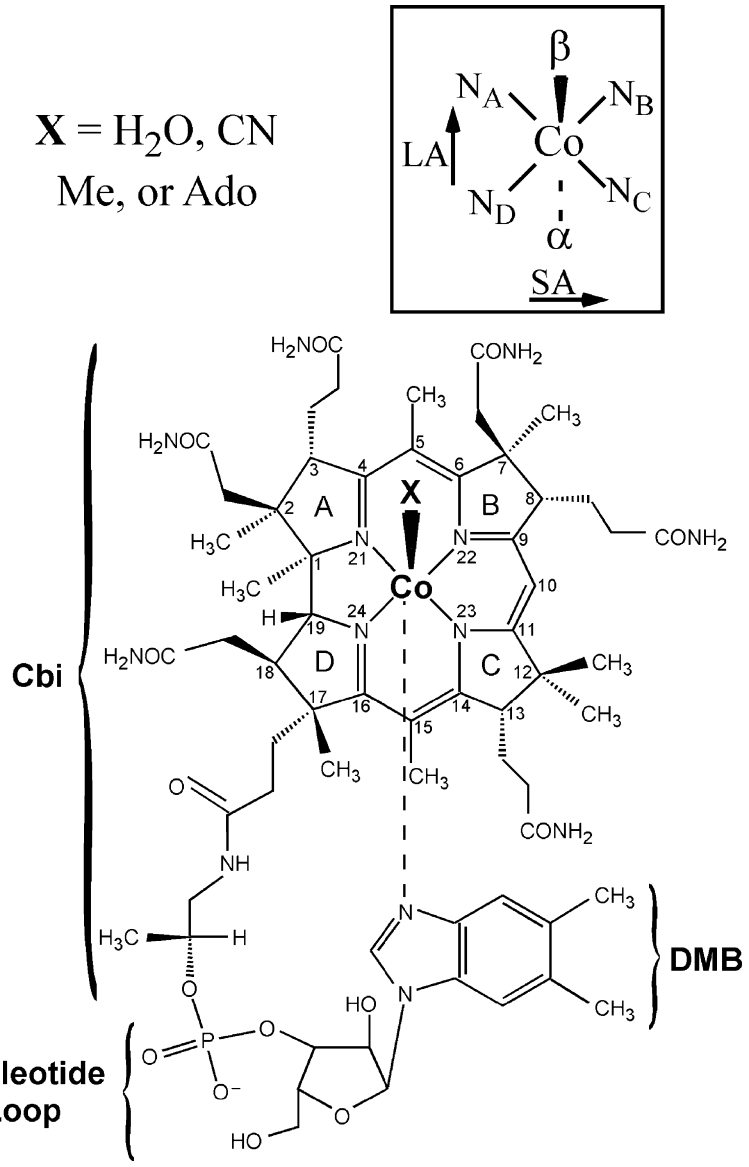

Fig. 1. Chemical structure and numbering scheme for Co^{3+}Cbl. The α ("lower") and β ("upper") faces of the cofactor and the short-axis (SA) and long-axis (LA) of the corrin macrocycle are defined in the inset. In aqueous solution, the coordination number of the Co ion is directly related to oxidation state. Upon reduction of Co^{3+}Cbl to Co^{2+}Cbl, the Co—X bond is cleaved. Further reduction of Co^{2+}Cbl to Co^{1+}Cbl breaks the axial Co—N bond. In cobinamides, the nucleotide loop including the DMB base is absent and a water molecule occupies the lower axial position in the Co^{3+} and Co^{2+} oxidation states (corresponding to Co^{3+}Cbi$^+$ and Co^{2+}Cbi$^+$, respectively).

By studying the electronic structures of a set of Co^{3+}Cbl cofactors whose β-axial ligands span a wide range of the spectrochemical series, significant insight has been obtained into the nature of the axial Co—C bonding interactions in AdoCbl and MeCbl, and viable strategies for enzymatic Co—C bond activation have been identified (*vide infra*).

Most DFT computational studies of Co^{3+}Cbl species have been carried out on truncated cofactor models that were derived from high-resolution X-ray crystallographic data [62–64] (notably, however, complete cofactor models have been used in two recent DFT studies of MeCbl [59] and AdoCbl [61]). Typically, the DMB base was modeled as an imidazole or an amine, the entire nucleotide loop was replaced by an H atom at C^{17} (see Fig. 1), and all other corrin ring substituents were replaced by H atoms. These truncated models were then either subjected to a DFT geometry optimization by minimizing the total electronic energy with respect to all atomic coordinates or used without further modifications. Although the former approach must be chosen for computing vibrational frequencies and normal mode compositions, our research revealed that the latter offers the advantage of preserving the actual conformation of the corrin ring by accounting for structural features not explicitly included in the cofactor models [26,27].

The interpretation of the vibrational (i.e., infrared, Raman, and rR) spectra of Co^{3+}Cbls has posed a significant challenge due to the low symmetry of the corrin macrocycle. Early studies revealed that the rR spectra of Co^{3+}corrinoids are dominated by features attributed to corrin ring vibrations [23,24]. The two most strongly enhanced modes were assigned to symmetric stretches polarized along the macrocycle's long-axis (LA, $Co\cdots C^{10}$ vector) and short-axis (SA, $C^5\cdots C^{15}$ vector) (Fig. 1), ν_{LA} and ν_{SA}, respectively, based upon their isotopic shifts in response to $^1H \rightarrow {}^2D$ labeling at C^{10}. Additionally, $^{12}C \rightarrow {}^{13}C$ isotopic labeling experiments in conjunction with rR studies by Spiro and co-workers led to the identification of vibrational features associated with the Co—C stretching modes, ν_{Co-C}, of AdoCbl and MeCbl [23,24] (note that in the case of AdoCbl, a subsequent DFT study by Kozlowski et al.

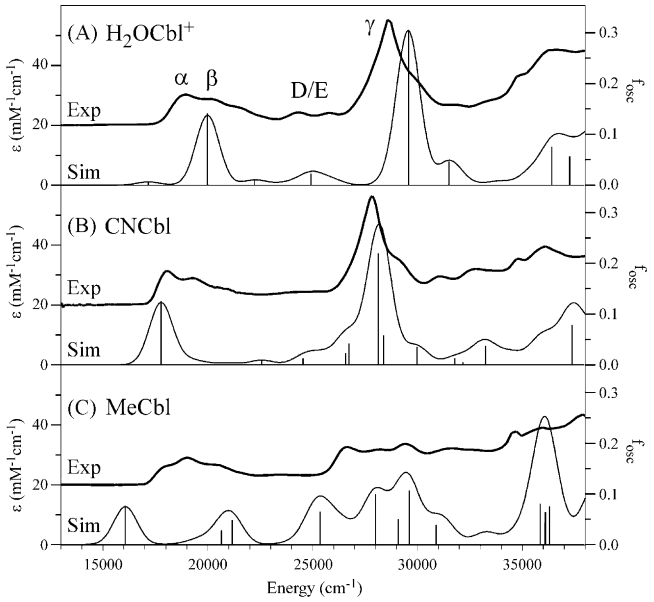

Fig. 2. Experimental and TDDFT-computed Abs spectra for H_2OCbl^+ (A), CNCbl (B), and MeCbl (C). The calculated spectra were uniformly red-shifted by 5500 cm^{-1} to facilitate comparison with the experimental data, which were obtained at 4.5 K. The transitions producing the dominant contributions to the calculated spectra are indicated by solid vertical lines (the corresponding oscillator strengths are given on the right-hand axis). Adapted from Ref. [26].

revealed that the original rR spectral assignments were incorrect because significant coupling occurs between the Co—C stretching and ribose deformation motions [57]). However, relatively little was known about the origin of the other vibrational features of Co^{3+}Cbls prior to the DFT-based analysis of the IR and Raman spectra of alkyl-Co^{3+}Cbl species by Kozlowski and co-workers [55]. These studies employed a DFT-scaled quantum mechanical force field that refined DFT-calculated force constants in order to compute vibrational frequencies and off-resonance Raman intensities [52]. Although somewhat poor agreement was achieved in the corrin stretching mode region (1450–1600 cm^{-1}), this force field satisfactorily reproduced the Co—C stretching mode region (350–650 cm^{-1}) of the Raman spectra of several alkyl-Co^{3+}Cbls and, therefore, provided a suitable basis to explore the origin of the different Co—C bond strengths in these species.

By utilizing Abs, CD, MCD, and rR spectroscopic techniques, an excellent framework was established for the validation of DFT-computed electronic structure descriptions for Co^{3+}Cbl species. Alternatively, DFT and TDDFT computational studies have played an important role in furthering our understanding of some of the subtleties of the experimental data. For the validation step, we have performed combined fits of the Abs, CD, and MCD data with a minimal number of Gaussian bands to determine the energies and Abs intensities of the dominant electronic transitions [26]. Furthermore, the polarizations of the major corrin-based $\pi \rightarrow \pi^*$ transitions were established on the basis of rR excitation profile studies, in which the relative intensities of the ν_{LA} and ν_{SA} modes were measured over a wide range of laser excitation wavelengths. Collectively, the insights gained in these experimental studies provided a suitable foundation to validate the calculated electronic structure descriptions for several Co^{3+}Cbl species on the basis of a comparison with the TDDFT-computed transition energies, oscillator strengths, and polarizations as obtained with the B3LYP hybrid functional [26,55,57,65–67].

Most Co^{3+}Cbl species, including H_2OCbl^+ and CNCbl, exhibit so-called "typical" Abs spectra (Fig. 2A and B) that are characterized by the presence of three diagnostic sets of features [68–70]: (i) the α/β-bands in the visible spectral region, assigned to the electronic origin and a vibrational sideband of an electronic excitation from the highest-occupied molecular orbital (HOMO) to the lowest-unoccupied molecular orbital (LUMO) of the corrin ring (i.e., a $\pi \rightarrow \pi^*$ transition) that is polarized along the macrocycle's long-axis; (ii) the D/E-bands, attributed to multiple corrin $\pi \rightarrow \pi^*$ transitions; and (iii) the prominent γ-band in the near-UV, assigned to a short-axis polarized corrin $\pi \rightarrow \pi^*$ transition. In contrast, alkyl-Co^{3+}Cbl species, such as MeCbl and AdoCbl, exhibit "unique" Abs spectra (Fig. 2C) that differ from the "typical" spectra (Fig. 2A and B) in several notable ways. While the α/β-bands still correspond to the electronic origin and a vibrational sideband associated with the long-axis polarized HOMO → LUMO ($\pi \rightarrow \pi^*$) transition of the corrin macrocycle, a second, similarly intense $\pi \rightarrow \pi^*$ transition contributes to this region of the "unique" Abs spectrum. The most striking difference, however, is that the intensity of the γ-band is redistributed over several similarly intense transitions in the near ultraviolet (UV) spectral region. Considering that all Co^{3+}Cbl Abs spectra are dominated by corrin $\pi \rightarrow \pi^*$ transitions, it seems rather puzzling that significant changes are observed upon upper axial ligand substitution. To explore the mechanism by which the axial ligands modulate the electronic properties of the corrin macrocycle (and, hence, the $\pi \rightarrow \pi^*$ transitions) and to identify the geometric and electronic factors distinguishing Co^{3+}Cbls displaying "typical" Abs spectra from those exhibiting "unique" spectra, we have performed DFT and TDDFT computations on a representative set of Co^{3+}Cbl species [26].

Fig. 2 shows a comparison between the experimental and TDDFT predicted Abs spectra for H_2OCbl^+, CNCbl, and MeCbl. Importantly, the computed spectra properly reproduce all of the salient features and trends observed experimentally, including the relative band positions and intensities, transition polarizations, progressive red-shift of the α/β-bands and the γ-band from H_2OCbl^+ to CNCbl and MeCbl, and the dramatic perturbation to the γ region upon coordination of an alkyl group in the upper axial position. This good agreement between experimental and computed Abs spectra warranted a more detailed interpretation of the computational results, in particular an analysis of the donor and acceptor molecular orbitals (MOs) involved in each transition.

In the case of H_2OCbl^+ and CNCbl, our TDDFT calculations confirmed that the α/β-bands are due to the corrin-based, long-axis polarized HOMO → LUMO ($\pi \rightarrow \pi^*$) transition and revealed that the γ region is dominated by a $\pi \rightarrow \pi^*$ transition that also originates from the HOMO of the macrocycle. The red-shift of the α/β-bands and the γ-band from H_2OCbl^+ to CNCbl (Fig. 2A and B) was found to reflect the greater σ-donor strength of the anionic CN^- ligand compared to H_2O. Specifically, more significant mixing occurs between the corrin π-based HOMO and the formally unoccupied Co $3d_{z^2}$ orbital in CNCbl, which induces a stronger σ-antibonding interaction between Co and the lower axial base. This increased antibonding interaction raises the energy of the HOMO, thus uniformly shifting all electronic transitions originating from this orbital to lower energy.

Because alkyl groups are even more potent σ-donor ligands than CN^-, the HOMOs of alkyl-Co^{3+}Cbls are subject to particularly large destabilizations, and the α/β-bands appear at lower energy in "unique" alkyl-Co^{3+}Cbl Abs spectra than in "typical" Co^{3+}Cbl spectra. Our DFT computational results for MeCbl further revealed that the increased σ-donor strength of the alkyl ligand also causes a net decrease in the effective nuclear charge of the Co^{3+} ion and, consequently, a large destabilization of all Co 3d orbitals. As a result, the occupied Co 3d-based MOs of MeCbl, and alkyl-Co^{3+}Cbls in general, shift closer in energy to the corrin-based HOMO, which gives rise to (i) a net increase in the number of donor MOs available for

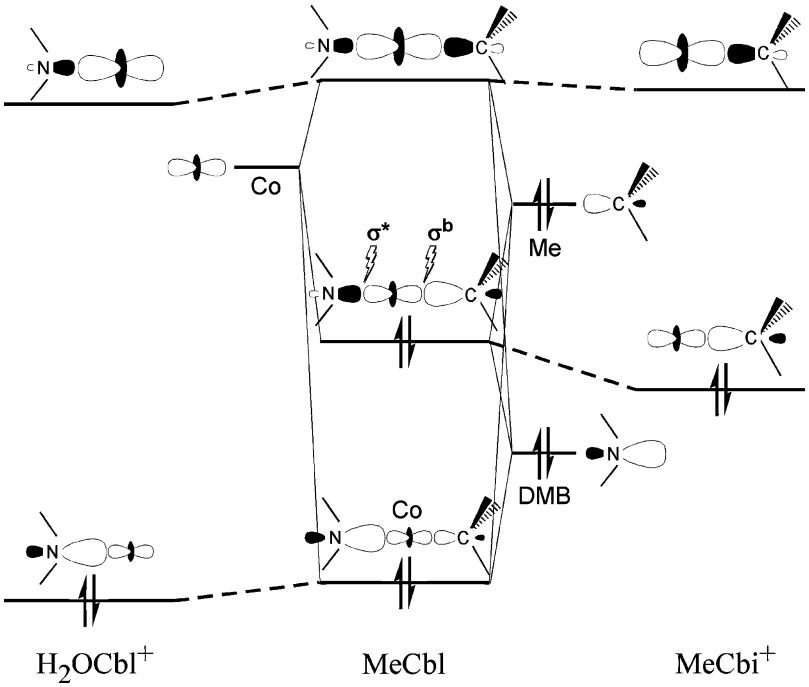

Fig. 3. Qualitative correlation diagram depicting the bonding interactions between the cobalt center and the axial ligands in H_2OCbl^+ (left), MeCbl (center), and $MeCbi^+$ (right). Adapted from Ref. [26].

electronic transitions and (ii) extensive mixing between Co 3d and corrin π orbitals. It is the combination of these two effects that is responsible for the "unique" Abs spectra of alkyl-Co^{3+}Cbls.

Our spectroscopically validated DFT computations also provided definitive clues as to why the identity of the upper axial ligand has a great effect on the Co—N (DMB) bond strength, whereas substitution of the lower axial ligand does not appreciably modulate the Co—C bond strength in alkyl-Co^{3+}Cbls. As depicted in the qualitative MO diagram in Fig. 3, replacement of the axial H_2O ligand of H_2OCbl^+ by a methyl group to generate MeCbl induces a substantial Co—N (DMB) σ-antibonding interaction and, consequently, causes a weakening of this bond. Alternatively, replacement of the lower axial DMB ligand of MeCbl by a water molecule in methylcobinamide ($MeCbi^+$) has virtually no effect on the Co—C bond order, and thus the bond strength, since in each case all occupied MOs are σ-bonding with respect to the Co—C bond. In support of this model, X-ray crystallographic data show a much shorter Co—N (DMB) bond in H_2OCbl^+ (1.925 Å [63]) than in MeCbl (2.162 Å [64]), and rR experiments by Spiro and co-workers revealed that the Co—C bond strengths in MeCbl and $MeCbi^+$ are virtually identical [23].

In summary, this particular application of a combined spectroscopic and computational methodology yielded a comprehensive understanding of the relationships between the σ-donating ability of the axial ligands and the geometric, electronic, and spectral properties of Co^{3+}Cbls. Additionally, this study revealed that B_{12}-dependent enzymes are unlikely to utilize Co—C bond activation mechanisms involving the lower axial ligand (Fig. 3) and established an excellent framework to study the interactions between Co^{3+}Cbls and enzyme active sites (as discussed in Section 3).

2.2. Co^{2+}corrinoids

Co^{2+}Cbl and $Co^{2+}Cbi^+$ can be prepared by the one-electron reduction of Co^{3+}Cbl and $Co^{3+}Cbi^+$ species, respectively [71]. These species contain a five-coordinate, low-spin ($S = 1/2$) Co^{2+} ion that is coordinated equatorially by the four nitrogens of the corrin macrocycle and axially ligated by either the tethered DMB base (in Co^{2+}Cbl) or a water molecule (in $Co^{2+}Cbi^+$) [4]. Co^{2+}corrinoid species have been shown to serve as intermediates in the catalytic cycles of B_{12}-dependent enzymes as well as during the biosynthesis of AdoCbl [72]. For instance, in AdoCbl-dependent isomerases, such as MMCM, an Ado•/Co^{2+}Cbl radical pair is generated by Co—C(Ado) bond homolysis [73–78]. In the case of MeCbl-dependent methyltransferases, such as MetH [79,80], a Co^{2+}Cbl species is occasionally formed via the accidental oxidation of the Co^{1+}Cbl reaction intermediate [47,81–83]. Finally, during AdoCbl biosynthesis, a Co^{2+}Cbl intermediate is produced during the step-wise reduction of Co^{3+}Cbl precursors to the Co^{1+}Cbl state [43,84–86].

The goal of developing a detailed understanding of how enzyme active sites modulate the geometric and electronic properties of Co^{2+}corrinoids has generated demand for a theoretical framework that can correlate observed spectroscopic changes to structural perturbations of the cofactor. Although DFT seemed well suited to achieve this goal, the fact that the computational results depend strongly on the choice of basis sets, functional, and initial geometry prompted us to perform a series of DFT computations on several cofactor models [27]. Specifically, we constructed three different models for free Co^{2+}Cbl and $Co^{2+}Cbi^+$ and employed two distinct density functionals to predict the corresponding Abs and EPR spectra using TDDFT and the coupled-perturbed SCF (CP-SCF) approach, respectively [27,87]. All models were based on the X-ray crystal structure coordinates of Co^{2+}Cbl and the same truncation scheme as described above for the Co^{3+}Cbl models (Section 2.1). Two of the three Co^{2+}Cbl models were then subjected to full DFT geometry optimizations using either the Vosko–Wilk–Nusair local density approximation [88] along with the nonlocal gradient corrections by Becke [66] and Perdew [89] for exchange and correlation, respectively, or Becke's three-parameter hybrid functional for exchange [67,90] along with the Lee–Yang–Par correlation functional [65] (B3LYP), while the remaining model was used without further modification so as to preserve the proper conformation of the corrin ring. The $Co^{2+}Cbi^+$ models were prepared in an analogous manner, except that the axially bound imidazole group was replaced with a water molecule, whose position was optimized in all three

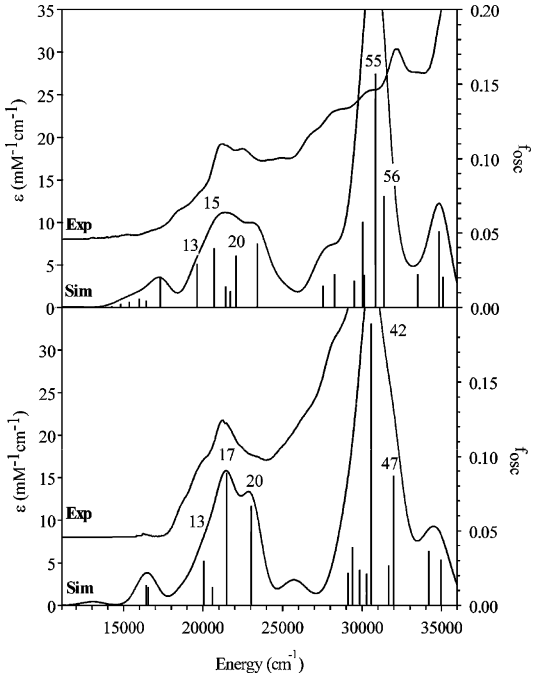

Fig. 4. Experimental and TDDFT-computed Abs spectra for Co^{2+}Cbl (top) and Co^{2+}Cbi$^+$ (bottom). The calculated spectra were uniformly red-shifted by 4000 cm^{-1} to facilitate comparison with the experimental data, which were obtained at 4.5 K. The transitions producing the dominant contributions to the calculated spectra are indicated by solid vertical lines (the corresponding oscillator strengths are given on the right-hand axis). Adapted from Ref. [27].

models. As expected, the corrin ring adopted a more planar conformation in all of the DFT-optimized models; yet, this flattening of the macrocycle had a relatively small effect on the axial ligand–Co bond length.

Two sets of TDDFT calculations were then performed on each Co^{2+}corrinoid model [27], one using the Perdew–Wang local density approximation (PW-LDA) [91] with the gradient corrections by Becke [66] and Perdew [89] and the other employing the B3LYP hybrid functional [65]. Although all TDDFT computations reproduced the key features in the experimental Abs spectra of Co^{2+}Cbl and Co^{2+}Cbi$^+$ reasonably well, the most satisfactory agreement was obtained with the PW-LDA functional using the non-optimized cofactor models (Fig. 4). Importantly, this set of TDDFT computations also properly predicted a small blue-shift of the dominant Abs feature in the visible spectral region from Co^{2+}Cbl to Co^{2+}Cbi$^+$ (note that in the following we refer to this feature as the α-band because it arises from the same corrin-based HOMO → LUMO ($\pi \rightarrow \pi^*$) transition as the α-band in the Co^{3+}Cbl Abs spectra). Contrary to the results obtained in these TDDFT calculations, better agreement between the experimental and DFT/CP-SCF-computed EPR parameters was achieved with the B3LYP functional regardless of the Co^{2+}corrinoid model used (Table 1). Because the computed EPR parameters were found to be relatively insensitive to the choice of cofactor model, the non-optimized structures could be used to explore both the ground state and the excited-state properties of Co^{2+}Cbl and Co^{2+}Cbi$^+$. Our finding that two distinct functionals are best suited for calculating Abs spectra and EPR parameters for Co^{2+}corrinoids is not necessarily surprising, because Abs spectroscopy probes the excited-state electronic structure of the cofactor, whereas EPR spectroscopy provides detailed information about the ground state wavefunction.

After using our spectroscopic data as the basis for establishing the best combinations of cofactor model and density functional, we utilized DFT computations to develop experimentally validated

Table 1
Computed and experimental EPR g values and hyperfine coupling constants (MHz) for Co^{2+}corrinoids. Adapted from Ref. [27].

	g_x	g_y	g_z	A_x(Co)	A_y(Co)	A_z(Co)	$A_{iso}(N_{ax})$
Co^{2+}Cbl							
CP-SCF	2.164	2.137	2.006	−24	30	435	50
Exp[a]	2.230	2.272	2.004	30	40	305	48
Co^{2+}Cbi$^+$							
CP-SCF	2.218	2.193	2.007	134	172	535	NA
Exp[b]	2.320	2.320	1.997	213	213	395	NA

[a] See Ref. [30].
[b] See Ref. [169].

electronic structure descriptions for Co^{2+}Cbl and Co^{2+}Cbi$^+$ and to explore the origin of the key differences between the corresponding Abs, MCD, and EPR spectra [27]. As shown in Fig. 4, the experimental Abs spectra of Co^{2+}Cbl and Co^{2+}Cbi$^+$ are almost superimposable, indicating that substitution of the DMB ligand by a water molecule only slightly perturbs the donor and acceptor MOs involved in the dominant electronic transitions (including the one responsible for the α-band). Consistent with this finding, our TDDFT calculations and analysis of the DFT-computed MO descriptions revealed that the visible region of the Co^{2+}corrinoid Abs spectra is dominated by transitions between corrin-based MOs, the compositions of which are nearly identical for Co^{2+}Cbl and Co^{2+}Cbi$^+$. In particular, none of these MOs have any significant contribution from the Co $3d_{z^2}$ orbital, which is the most strongly affected orbital by axial ligand substitution because it points directly toward the axial coordinated sites. Note that the low sensitivity of the corrin $\pi \rightarrow \pi^*$ transitions to perturbations in the axial bonding scheme of Co^{2+}corrinoids is in marked contrast to the situation encountered for Co^{3+}corrinoids, whose Abs spectra vary distinctively depending on the identity of the axial ligands (*vide supra*).

Compared to Abs spectra, MCD data provide significantly deeper insight into the electronic structures of the paramagnetic ($S = 1/2$) Co^{2+}corrinoids, even enabling the observation of ligand field (LF) transitions that are formally electric-dipole forbidden and thus too weak to be discerned by Abs spectroscopy [92]. While the Abs spectra of Co^{2+}Cbl and Co^{2+}Cbi$^+$ are nearly indistinguishable, the positions and relative intensities of the low-energy features in the corresponding MCD spectra vary dramatically in response to axial ligand substitution (Fig. 5) [27]. Our DFT and TDDFT results revealed that this region of the MCD spectra of Co^{2+}corrinoids is indeed dominated by LF transitions. Hence, MCD spectroscopy offers an almost ideal probe of the cobalt ligand environment in Co^{2+}Cbl and Co^{2+}Cbi$^+$. The significance of this finding will become particularly apparent in our discussion of the interaction between Co^{2+}corrinoids and enzyme active sites (Sections 3.1–3.3).

Our DFT/CP-SCF calculations for Co^{2+}corrinoids using the B3LYP hybrid functional have enabled an MO-based interpretation of the EPR parameters obtained experimentally (Table 1) [27]. As expected on the basis of qualitative considerations, these computations confirmed that the larger $A(^{59}Co)$ hyperfine values observed for Co^{2+}Cbi$^+$ than for Co^{2+}Cbl reflect an increase (by ∼5%) in the unpaired spin density residing on the Co^{2+} center in the former species. This result can be attributed to a decrease in covalent character of the axial ligand–Co bond when the DMB moiety is replaced by a water molecule. Our DFT/CP-SCF calculations further revealed that the increase in the g_x and g_y values from Co^{2+}Cbl to Co^{2+}Cbi$^+$ can be explained in terms of a weaker bonding interaction of the cobalt center with a water molecule than with the DMB moiety. This weakened interaction leads to a sizable stabilization of the Co $3d_{z^2}$ orbital, which is σ-antibonding with respect to the axial ligand–Co bond, and thus to a substantial increase in spin–orbit

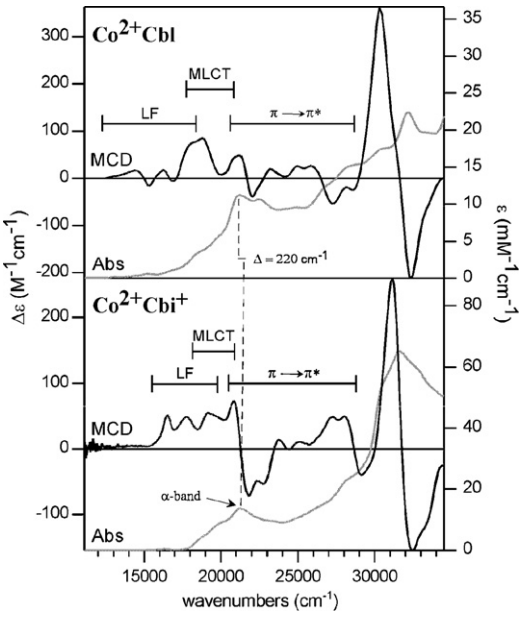

Fig. 5. 7 T MCD (black traces, left-axis) and Abs (grey traces, right-axis) spectra collected at 4.5 K of Co^{2+}Cbl (top) and Co^{2+}Cbi$^+$ (bottom). Adapted from Ref. [27].

mixing between the Co $3d_{xz} \rightarrow 3d_{z^2}$ and $3d_{yz} \rightarrow 3d_{z^2}$ LF excited states and the ground state. This increased orbital angular momentum in the ground state gives rise to the larger g_x and g_y values for Co^{2+}Cbi$^+$ relative to Co^{2+}Cbl.

Collectively, our combined spectroscopic/computational studies of Co^{2+}Cbl and Co^{2+}Cbi$^+$ provided significant new insight into the spectral and electronic properties of these species. Additionally, they established an excellent framework to interpret spectral changes accompanying Co^{2+}corrinoid binding to enzyme active sites in terms of geometric perturbations to the cofactor, as described in Sections 3.1–3.3.

2.3. Co^{1+}corrinoids

The "superreduced" form of the B_{12} cofactor, Co^{1+}Cbl, is utilized by several enzymatic systems relevant to human health and environmental remediation [93–95]. MetH utilizes Co^{1+}Cbl as a catalytic intermediate during methyl-group transfer from CH_3THF to Hcy [46,47]. This reaction is essential to avoid the accumulation of Hcy and CH_3THF in the cell, the consequences of which would be hyperhomocystinuria and megaloblastic anemia, respectively [46,96,97]. Co^{1+}Cbl is also a reactive intermediate during the MetH activation process in which the inactive Co^{2+}Cbl form of the cofactor is converted to MeCbl [98]. Similarly, a Co^{1+}Cbl intermediate is formed in the catalytic cycles of ATR enzymes that catalyze the Co—C bond formation step in the biosynthesis of AdoCbl [43–45,94]. Lastly, the Co^{1+}Cbl oxidation state is also used by the reductive dehalogenases, a class of enzymes that reductively cleave the carbon–halogen bonds of a wide range of halogenated organic substrates [95]. This enzymatic process is attractive from both fundamental and environmental points of view, because biodegradation could potentially be exploited for the decontamination of sites polluted by halogenated hydrocarbons.

Several research groups have contributed to a growing library of spectroscopic data for free Co^{1+}Cbl [28,56,99–101]. Although this species has thus far eluded characterization by X-ray crystallography, presumably due to its extreme sensitivity to molecular oxygen, analyses of X-ray absorption spectroscopy (XAS) and extended XAS fine structure data have revealed that Co^{1+}Cbl contains a four-coordinate, approximately square-planar cobalt center with an average Co—N bond length of 1.86–1.88 Å [102,103]. rR studies in conjunction with isotopic labeling experiments permitted the identification of several corrin-based modes between 1450 and 1600 cm^{-1} [13,14,28]. More recently, the electronic structure of Co^{1+}Cbl has been extensively investigated by Abs, CD, and MCD spectroscopic techniques [28,104]. Collectively, these spectroscopic studies have afforded a wealth of information about the geometric and electronic properties of Co^{1+}Cbl, thereby establishing an excellent framework for the validation of DFT computations.

DFT geometry optimizations with either the Vosko–Wilk–Nusair-5 LDA (VWN5-LDA) along with the Perdew–Burke–Ernzerhof (PBE) generalized gradient approximation for exchange and correlation [88,105] or the B3LYP hybrid functional [65] and a model of Co^{1+}Cbl that was generated using the same truncation scheme as the one employed for the Co^{3+}Cbl and Co^{2+}Cbl models described above yielded average Co—N bond lengths of 1.87 and 1.88 Å, respectively [28,101,105], in excellent agreement with the structural parameters derived from XAS spectroscopic studies of this species [102,103]. Both of these optimized models were found to possess relatively planar corrin ring conformations, as expected on the basis of the fact that the Co^{1+} center of the Co^{1+}Cbl species lacks any axial bonding interactions. Consequently, all currently available structural data for Co^{1+}Cbl suggest that the truncated model used in these DFT studies accurately mimics the geometry of the actual cofactor in its "superreduced" state.

Starting from the optimized Co^{1+}Cbl model obtained with the PBE functional, the effects of two structural modifications on the overall geometry of the cofactor were investigated by additional DFT computations [28]. First, a water molecule was placed 2.2 Å away from the Co^{1+} center in an axial position and the geometry was re-optimized using the PBE functional. In the course of this optimization, the water molecule moved away from the Co^{1+} center and rotated so as to form a weakly bound complex via one of its H atoms. However, consistent with all available experimental data, this complex was found to be unstable toward decomposition into H_2O and four-coordinate Co^{1+}Cbl based on the computed standard Gibbs free energy for the decomposition reaction of −1.96 kcal/mol *in vacuo*. Second, the methyl groups and side-chains were appended to the truncated Co^{1+}Cbl model to form a complete model of Co^{1+}Cbi$^+$, which differs from the actual Co^{1+}Cbl cofactor by the lack of the nucleotide loop and DMB base (note that the Co^{1+} coordination environments in these two species should be identical because the DMB moiety no longer coordinates to the cobalt center in the fully reduced state of the cofactor). A comparison of the DFT geometry-optimized structures of the complete Co^{1+}Cbi$^+$ model and its precursor, the truncated Co^{1+}Cbl model, revealed essentially no differences in the average Co—N bond lengths and only a slightly more pronounced corrin ring fold in the larger model. This result implies that the geometry of the actual Co^{1+}Cbl cofactor is almost entirely controlled by the atoms included in the truncated model. It should be noted, however, that the side chains are likely to play an important role in properly orienting the cofactor in enzyme active sites.

The moderate size and good mimicry of the actual cofactor structure also permitted us to use the truncated Co^{1+}Cbl model in a DFT-based vibrational frequency calculation aimed at assigning the corrin-based modes between 1450 and 1650 cm^{-1} (Fig. 6) that dominate the experimental rR spectra of this species [28]. Of the numerous features that are observed in this frequency range of the Co^{1+}Cbl rR spectra, three bands display a particularly large enhancement upon laser excitation in resonance with the prominent Abs features in the visible spectral region (Fig. 7, top). Consistent with this experimental finding, the DFT vibrational frequency calculation with the PBE functional predicted three

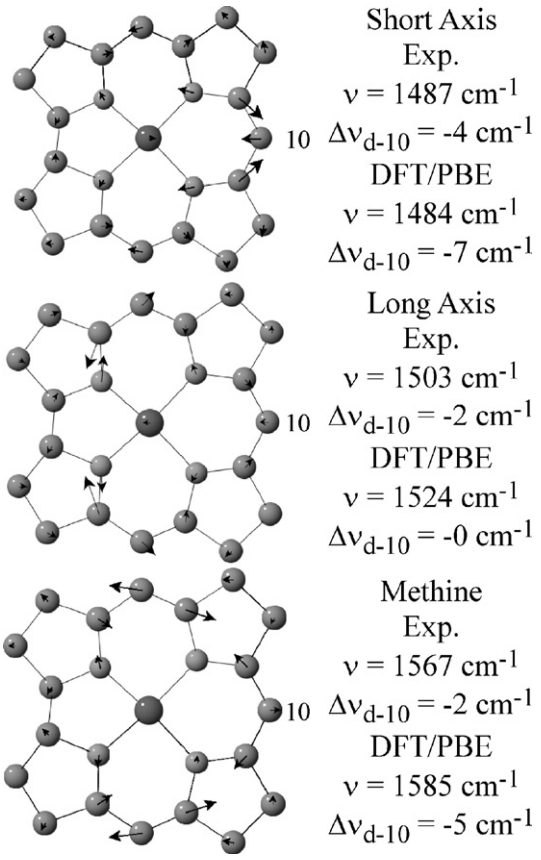

Fig. 6. DFT-computed eigenvector representations of the totally symmetric corrin-based stretching modes for Co^{1+}Cbl. Their computed frequencies (ν) and downshifts in response to H → D exchange at C^{10} ($\Delta\nu_{d\text{-}10}$) are shown on the right. Adapted from Ref. [28].

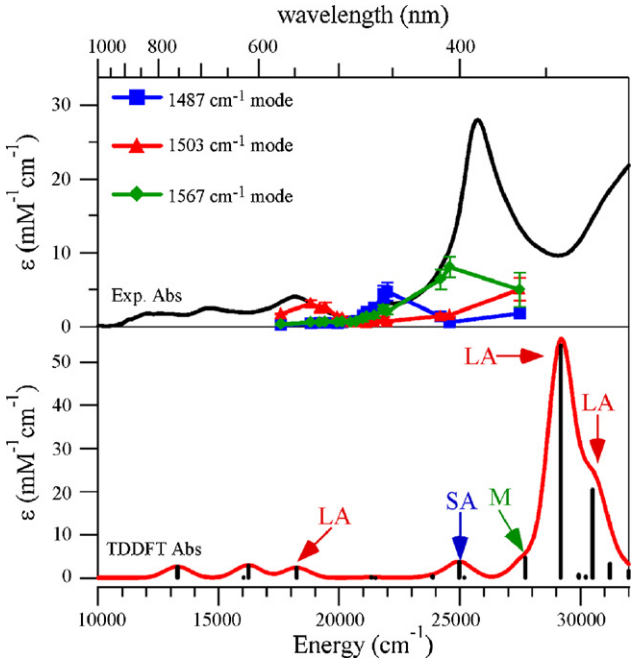

Fig. 7. Top: 4.5 K Abs spectrum and 77 K rR profile of Co^{1+}Cbl. Bottom: TDDFT-computed Abs spectrum and rR enhancement patterns inferred from DFT-computed MO descriptions for Co^{1+}Cbl. Adapted from Ref. [28].

totally symmetric corrin-based stretching modes with frequencies between 1450 and 1600 cm^{-1} (Fig. 6). Additionally, the computed downshifts upon $^1H \rightarrow {}^2D$ isotopic labeling at C^{10}, $\Delta\nu_{d\text{-}10}$, were found to agree reasonably well with those observed experimentally for these three modes. This good correspondence between experimental and DFT-predicted rR data warranted the use of these computational results as the basis for developing specific assignments of the three most strongly resonance-enhanced normal modes of vibration of Co^{1+}Cbl.

The largest downshift upon $^1H \rightarrow {}^2D$ exchange at C^{10}, both observed experimentally and predicted computationally, is associated with the ~1485 cm^{-1} vibrational feature, which is therefore assigned to the short-axis stretch of the corrin macrocycle (Fig. 6, top). Similarly, on the basis of their frequencies and $\Delta\nu_{d\text{-}10}$ values, the remaining two corrin-based totally symmetric stretching modes in this region, observed at 1503 and 1567 cm^{-1} in the experimental rR data, were assigned to the long-axis and methine stretches, respectively. As all three of these corrin-based normal modes primarily involve nuclear displacements within the plane of the macrocycle, their frequencies can potentially be depressed by substituents attached to the periphery of the corrin ring, especially the two methyl groups at C^5 and C^{15} (Fig. 1) that are located within the corrin ring plane. Because these methyl groups were replaced by hydrogen atoms in our truncated Co^{1+}Cbl model, it is not surprising that our DFT computation overestimated the frequencies of the symmetric long-axis and methine stretches, both of which involve a significant movement of the C^5 and/or C^{15} carbons, but not of the symmetric short-axis stretch (see Fig. 6).

The combination of PBE functional and truncated Co^{1+}Cbl model also proved to be well suited for an analysis of the Abs spectrum of the "superreduced" form of the B_{12} cofactor [28]. To extract the energies and Abs intensities of the dominant electronic transitions of Co^{1+}Cbl, we performed combined fits of the corresponding Abs, CD, and MCD spectra with the minimal number of Gaussian bands needed to replicate the main features of the experimental spectra. This analysis revealed that the TDDFT-computed Abs spectrum for Co^{1+}Cbl not only provided an accurate reproduction of the experimental Abs trace (Fig. 7) but also yielded almost quantitative agreement with the electronic transition energies and Abs intensities derived from our spectral fits. Additionally, our TDDFT computation provided a description of the donor and acceptor MOs for each electronic transition that was found to be consistent with the observed rR enhancement behavior of the three totally symmetric corrin-based stretching modes in the 1450–1600 cm^{-1} frequency range (Fig. 6). Because of this good agreement between our Abs, CD, MCD, and rR spectroscopic data and our computational results, a more detailed analysis of the DFT-computed MO descriptions for our Co^{1+}Cbl model was warranted [28].

As shown in Fig. 8, the highest-energy corrin π-based MO of Co^{1+}Cbl is nearly 1.5 eV lower in energy than the Co $3d_{xz}$-, $3d_{yz}$-, and $3d_{z^2}$-based orbitals. Furthermore, the three lowest-energy unoccupied MOs are all corrin π*-based. These observations provide a rationale for the TDDFT-based assignment of the four moderately intense low-energy features in the Abs spectrum of Co^{1+}Cbl (Fig. 7) to Co 3d → corrin π* charge transfer transitions. The major Abs feature in the near-UV region was attributed to a corrin-centered π → π* excitation (involving MOs π_7 and π_8* in Fig. 8) that corresponds to the HOMO → LUMO transition of the metal-free corrin macrocycle. Hence, this transition is very similar in nature to the one responsible for the α-band in the Abs spectra of Co^{3+}Cbl species. While interesting in the context of the spectral and electronic properties of the free cofactor alone, these specific band assignments will be particularly useful for correlating changes in the electronic spectra of Co^{1+}Cbl upon binding to a given enzyme active site with

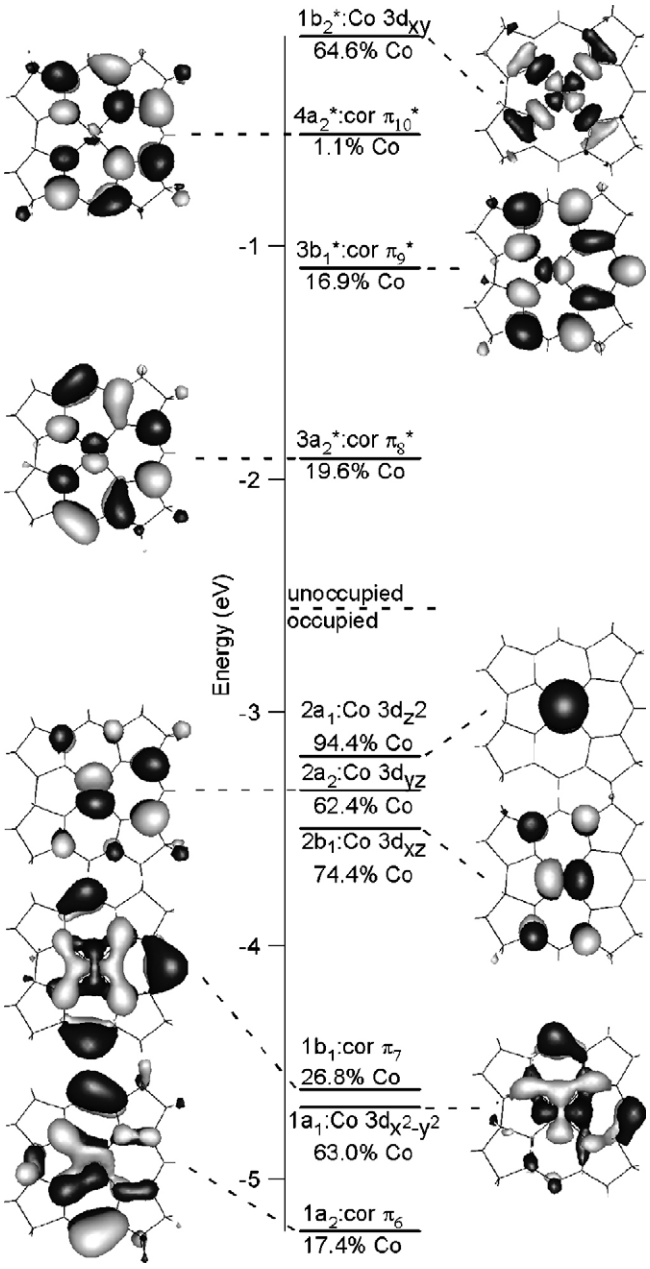

Fig. 8. DFT-computed MO diagram for Co^{1+}Cbl, with the approximate C_{2v} symmetry labels and percent contributions from the Co 3d orbitals. Adapted from Ref. [28].

perturbations to the geometric and electronic structures and, thus, the nucleophilicity of this species.

3. Enzyme-bound B_{12}

3.1. ATP: corrinoid adenosyltransferases

Regardless of whether AdoCbl is synthesized *de novo* or derived from an externally salvaged source, a class of enzymes termed ATRs are utilized to catalyze the formation of the cofactor's Co—C(Ado) bond through the transfer of the Ado group from a molecule of ATP to a transient Co^{1+}corrinoid species generated in the enzyme active site (Fig. 9) [86,94,106]. A particularly puzzling aspect of this reaction is that the $Co^{2+/1+}$corrinoid reduction midpoint potential is substantially lower than the E° values of putative *in vivo* reducing agents; e.g., for unbound Co^{2+}Cbl and

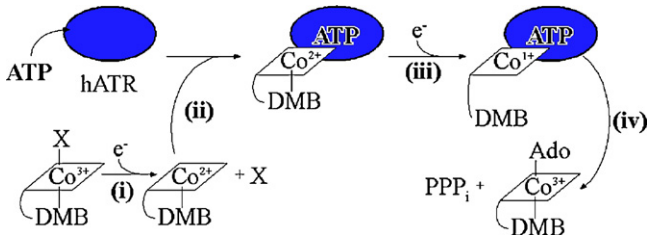

Fig. 9. Proposed mechanism for cobalamin adenosylation catalyzed by hATR. Assimilated cobalamin (X = H_2O, CN^-, etc.) is reduced to Co^{2+}Cbl (i) that then binds to the hATR/ATP complex (ii). Further reduction yields a nucleophilic four-coordinate Co^{1+} intermediate (iii) that attacks the 5′-carbon of the co-substrate ATP to generate AdoCbl and tripolyphosphate (iv). Adapted from Ref. [111].

$Co^{2+}Cbi^+$, $E^{\circ} = -610$ and -490 mV vs. SHE, respectively, while for the semiquinone/hydroquinone couple of the flavin cofactor of flavodoxin A, $E^{\circ} = -440$ mV [107–109]. Therefore, the mechanism by which ATRs accomplish the thermodynamically challenging $Co^{2+} \rightarrow Co^{1+}$ reduction has been the subject of considerable research interest.

Three evolutionarily distinct classes of ATRs can be distinguished; namely, the CobA, PduO, and EutT families of enzymes. The interactions of both Co^{2+}Cbl and $Co^{2+}Cbi^+$ with different members of the CobA- and PduO-type ATRs have been examined in detail with Abs, MCD, and EPR spectroscopic techniques [110–112]. Given that these enzymes catalyze the formally endergonic $Co^{2+} \rightarrow Co^{1+}$ reduction, it is not surprising that rather drastic spectral changes were noted upon binding of the Co^{2+}corrinoid substrates to ATRs complexed with co-substrate ATP. In the case of the CobA-type ATR obtained from *Salmonella enterica* [110], binding of $Co^{2+}Cbi^+$ to the enzyme active site led to the appearance of a pair of positively signed, intense features at 12 340 and 20 320 cm^{-1} in the MCD spectrum (Fig. 10) and to a small blue-shift of the α-band in the Abs spectrum (not shown). Similarly drastic changes accompanying $Co^{2+}Cbi^+$ binding to the CobA/ATP complex were observed by EPR spectroscopy; most notably, the appearance of a series of widely spread resonances in the low-field region. A simulation of this EPR spectrum required much larger g_2, g_3, and $A(^{59}Co)$ hyperfine

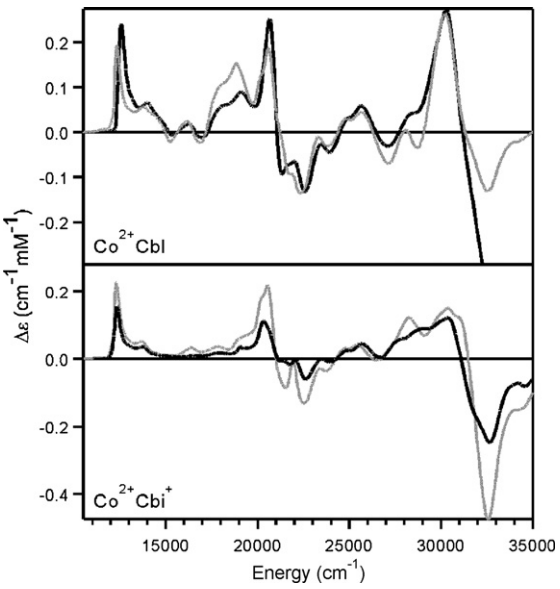

Fig. 10. Top panel: 4.5 K MCD spectra of Co^{2+}Cbl bound to the hATR/ATP complex (solid black line [111]) and the PduO/ATP complex (dotted gray line [112]). Bottom panel: 4.5 K MCD spectra of $Co^{2+}Cbi^+$ bound to the CobA/ATP complex solid black line [110]) and the PduO/ATP complex (dotted gray line [112]).

Table 2
EPR g values and $A(^{59}Co)$ hyperfine coupling constants (in MHz) from the spectral fits presented in [110–112], which were performed using the WEPR program developed by Dr. Frank Neese [170].

	g_1	g_2	g_3	$A_1(^{59}Co)$	$A_2(^{59}Co)$	$A_3(^{59}Co)$
Co^{2+}Cbl	2.004	2.230	2.280	305	30	40
Co^{2+}Cbi$^+$	1.999	2.338	2.338	405	220	220
Co^{2+}Cbi$^+$ + CobA/ATP	2.060	2.670	2.730	805	590	635
Co^{2+}Cbl + hATR/ATP	1.990	2.699	2.705	770	805	595
Co^{2+}Cbl + *Lr*PduO/ATP	1.990	2.700	2.720	770	755	595
Co^{2+}Cbi$^+$ + *Lr*PduO/ATP	1.990	2.650	2.740	810	665	565

values than those obtained from a fit of the free Co^{2+}Cbi$^+$ spectrum (Table 2), indicating that the Co^{2+} ligand environment of the enzyme-bound cofactor is considerably perturbed. Interestingly, similar results were obtained with all other ATRs studied to date. For example, the human ATR (hATR) [111], a PduO-type enzyme, perturbs the MCD and EPR spectra of Co^{2+}Cbl, its native substrate, in nearly the same way as CobA does for its substrate Co^{2+}Cbi$^+$, even though these two enzymes are structurally and evolutionary unrelated. Most recently, the PduO-type ATR from *Lactobacillus reuteri* was found to perturb the spectral properties of Co^{2+}Cbl and Co^{2+}Cbi$^+$ almost identically and in essentially the same manner as hATR and CobA, respectively, which correlates nicely with this enzyme's ability to adenosylate both Co^{2+}corrinoid substrates [112]. Collectively, these results suggest that ATRs employ a universal strategy for accomplishing $Co^{2+} \rightarrow Co^{1+}$ reduction, one that involves the formation of an "activated" Co^{2+}corrinoid intermediate exhibiting unique MCD and EPR spectral signatures.

To correlate the spectral changes accompanying Co^{2+}Cbl and Co^{2+}Cbi$^+$ binding to ATR enzyme active sites with geometric and electronic perturbations of the cofactor, we have employed DFT and TDDFT computational methods. On the basis of the insights gained from our studies of free Co^{2+}corrinoids (Section 2.2) [27], we speculated that the spectral signatures of the "activated" Co^{2+}corrinoid intermediate reflect a significantly perturbed axial ligand environment of the Co^{2+} center. To test this hypothesis, we generated a series of perturbed Co^{2+}Cbi$^+$ models for which the Co—OH_2 bond was systematically lengthened in increments of 0.05 Å from the equilibrium distance of 2.20 Å while the coordinates of all other atoms were kept fixed. The effect of this structural perturbation on the spectral properties of Co^{2+}Cbi$^+$ was then evaluated by TDDFT Abs spectrum and DFT/CP-SCF EPR parameter calculations [110]. To assess the feasibility of this computational approach, we first carried out TDDFT and DFT/CP-SCF calculations on a structurally and spectroscopically well-characterized model complex of Co^{2+}Cbi$^+$, [Co(Me$_6$[14]dieneN$_4$)(H_2O)] (Fig. 11; see figure caption for full name) [113,114]. Importantly, these computational studies of [Co(Me$_6$[14]dieneN$_4$)(H_2O)] revealed that TDDFT calculations using the PW-LDA functional consistently overestimate the energies of the Co^{2+} LF transitions by ~6500 cm^{-1}. Additionally, DFT/CP-SCF EPR parameter calculations for [Co(Me$_6$[14]dieneN$_4$)(H_2O)] and the Co^{2+}Cbi$^+$ model using the PW-LDA functional [27] indicated that this approach tends to underestimate the g_x and g_y values and overestimate the $A(^{59}Co)$ hyperfine coupling constants relative to the experimentally obtained values [114]. Based on these findings, which permitted us to suitably adjust the TDDFT-computed LF transition energies for the Co^{2+}Cbi$^+$ model, we were able to conclude that the lowest-energy feature at ~16 000 cm^{-1} in the MCD spectrum of free Co^{2+}Cbi$^+$ (Fig. 5, bottom) corresponds to the Co $3d_{xy} \rightarrow 3d_{z^2}$ transition, whereas the Co $3d_{xz} \rightarrow 3d_{z^2}$ and $3d_{yz} \rightarrow 3d_{z^2}$ transitions occur below 9000 cm^{-1} and thus outside the range accessible by our MCD instrument.

Building upon the theoretical foundation established in our computational studies of [Co(Me$_6$[14]dieneN$_4$)(H_2O)] and free Co^{2+}Cbi$^+$, we subsequently performed TDDFT and DFT/CP-SCF calculations on the perturbed Co^{2+}Cbi$^+$ models with differing Co—OH_2 bond lengths. The TDDFT computational results suggested that the dominant feature in the visible region of the Abs spectrum of Co^{2+}Cbi$^+$ (the α-band) blue-shifts by ~15 cm^{-1}/pm as the Co—OH_2 bond length is increased from its equilibrium value. The reason for this predicted band shift is that even though the donor MO involved in the corresponding transition is mostly corrin π-based, it also possesses significant Co $3d_{z^2}$-orbital character and a small contribution from a lone pair of the H_2O ligand, making it weakly Co—OH_2 σ-antibonding. As the Co—OH_2 bond is elongated, this σ-antibonding interaction becomes weaker and the corresponding MO is stabilized in energy, thereby causing a blue-shift of the α-band. However, the most dramatic perturbation to the electronic structure of Co^{2+}Cbi$^+$ in response to a lengthening of the Co—OH_2 bond involves the Co 3d-based MOs that are responsible for the low-energy features in the experimental MCD spectrum (Fig. 5, bottom). In particular, a weakening of the Co—OH_2 σ-antibonding interaction was found to stabilize MOs with significant Co $3d_{z^2}$ orbital character, giving rise to considerable red-shifts of LF transitions terminating in these orbitals. This prediction that certain transitions shift toward lower energy upon weakening of the Co—OH_2 bonding interaction afforded a straightforward explanation for the apparent red-shift (from ~16 500 to 12 500 cm^{-1}) of the lowest-energy discernible MCD feature of Co^{2+}Cbi$^+$, assigned to the Co $3d_{xy} \rightarrow 3d_{z^2}$ transition, upon cofactor binding to the CobA/ATP complex (Fig. 10, bottom). Consequently, our DFT- and TDDFT-based spectral analysis suggested that CobA induces a significant lengthening of the cofactor's Co—OH_2 bond. Based on the striking similarities between the MCD spectra of all "activated" Co^{2+}corrinoids studied to date (Fig. 10), this strategy is likely shared by many members of the ATR family of enzymes.

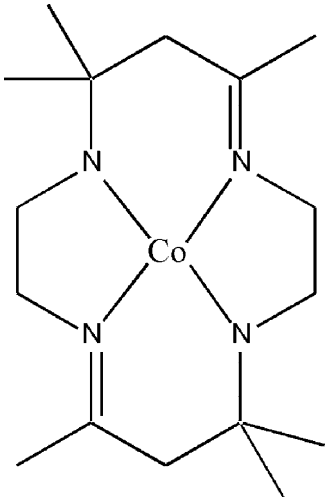

Fig. 11. Chemical structure of [Co^{2+}-5,7,7,12,14,14-hexamethyl-1,4,8,11-tetraazacyclotetradeca-4,11-diene(H_2O)], abbreviated by [Co(Me$_6$[14]dieneN$_4$)] in the text.

Similar to the LF transition energies that can be probed by MCD spectroscopy, the EPR g values of $Co^{2+}Cbi^{+}$ are also extremely sensitive to the Co—OH_2 bond length. A lengthening of this bond stabilizes the Co $3d_{z^2}$-based MO and thus allows for more efficient spin–orbit mixing of Co $3d_{xz} \rightarrow 3d_{z^2}$ and $3d_{yz} \rightarrow 3d_{z^2}$ excited-state character into the ground state, causing the g_2 and g_3 values to shift farther away from the free electron g value of 2.00 [115]. Additionally, the expected decrease in Co—OH_2 bond covalency accompanying elongation of this bond should lead to an increase in the unpaired spin density on the Co center and, in turn, the $A(^{59}Co)$ hyperfine coupling constants. These qualitative predictions, which were verified quantitatively by DFT/CP-SCF calculations on the perturbed $Co^{2+}Cbi^{+}$ models, concur nicely with the dramatic changes in g values and $A(^{59}Co)$ hyperfine parameters observed by EPR spectroscopy when Co^{2+}corrinoid substrates bind to the ATR/ATP complexes (Table 2).

Collectively, the results obtained in these combined spectroscopic and computational studies of the interaction between $Co^{2+}Cbl$ and $Co^{2+}Cbi^{+}$ and different ATR enzymes complexed with the co-substrate ATP provided conclusive evidence that the enzyme-bound Co^{2+}corrinoid species possess a substantially elongated Co—OH_2 bond. In fact, on the basis of the spectro/structural correlations we established by carrying out TDDFT and DFT/CP-SCF calculations on perturbed $Co^{2+}Cbi^{+}$ models with differing Co—OH_2 bond lengths, the Abs and EPR spectral changes observed experimentally were interpreted as indicating that these "activated" species contain an essentially four-coordinate, square-planar Co^{2+} complex with, perhaps, a very weakly interacting oxygen-based axial ligand. By imposing such an unusual coordination environment on their Co^{2+}corrinoid substrates, the ATR enzymes effectively achieve a substantial (>0.25 eV) stabilization of the Co $3d_{z^2}$-based redox-active MO, thereby raising the $Co^{2+/1+}$ reduction potential by an estimated ~250 mV from that of $Co^{2+}Cbi^{+}$ ($E^{\circ} = -490$ mV) and thus well into the range accessible to the putative *in vivo* reducing agents. Moreover, by forcing the Co^{2+}corrinoid substrates to adopt the preferred geometry of the corresponding Co^{1+}corrinoid "products", these enzymes ensure that the kinetic barrier for $Co^{2+} \rightarrow Co^{1+}$ reduction is minimal. Another noteworthy finding from these studies is that the "activated" Co^{2+}corrinoid species are formed in high yield only in the presence of co-substrate ATP. This prerequisite provides an elegant means by which the ATR enzymes can control the timing of $Co^{2+} \rightarrow Co^{1+}$ reduction so as to protect themselves from being attacked by the transiently formed Co^{1+}corrinoid "supernucleophile".

3.2. AdoCbl-dependent isomerases

The only AdoCbl-dependent enzyme found in humans is MMCM, which catalyzes the 1,2-rearrangement reaction of MMCoA to SCoA [33,116]. MMCM is a member of the family of AdoCbl-dependent isomerases, which also includes GM, diol dehydratase, and ethanolamine ammonia lyase, among others [117]. The reaction catalyzed by MMCM is essential for the catabolism of MMCoA; improper function of this enzyme leads to methylmalonic aciduria, an autosomal disorder that is often fatal in infants [118]. X-ray crystallographic studies of the bacterial *Propionibacterium shermanii* MMCM revealed that this enzyme crystallizes as a heterodimer of 80 and 69 kDa chains, termed the α and β subunits, respectively, with one AdoCbl molecule bound to the larger subunit [119]. The mammalian enzyme is a homodimer composed of two subunits that are highly homologous to the α-chain of the bacterial MMCM and, accordingly, contains two AdoCbl binding sites [120].

GM catalyzes the reversible interconversion of L-glutamate and L-threo-3-methylaspartate as the first step in the fermentation pathway of glutamate in some *Clostridia* [75,121]. The X-ray crystal structure of GM isolated from *Clostridium cochlearium* identified this enzyme as a heterotetramer of two larger ε subunits (~55 kDa) and two smaller σ subunits (~15 kDa), with a molecule of AdoCbl bound at each σ/ε subunit interface [122]. Although GM and MMCM are structurally and evolutionary unrelated, both enzymes share similar structural motifs responsible for binding AdoCbl and utilize a common TIM barrel motif that acts as the substrate-binding domain. Additionally, both enzymes induce a lower axial ligand switch upon binding of the AdoCbl cofactor to their active sites, replacing the intramolecular DMB with a protein-derived His residue (His610 in MMCM and His16 in GM) [119,122].

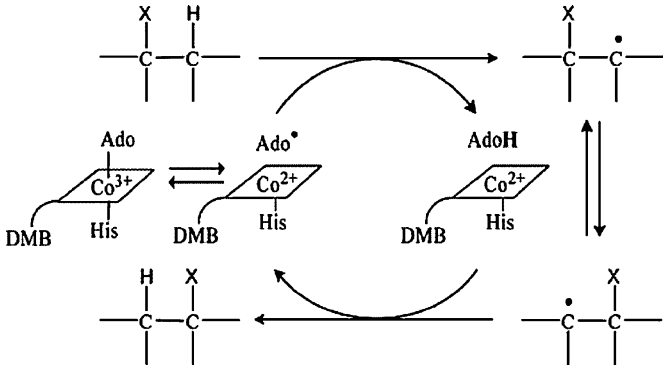

Fig. 12. Generic mechanism for AdoCbl-dependent isomerases. Adapted from [78].

The initial step common to the catalytic cycles of all AdoCbl-dependent isomerases (Fig. 12) involves homolytic cleavage of the Co—C(Ado) bond to generate $Co^{2+}Cbl$ and an organic radical centered on the 5′-carbon of the Ado moiety (Ado•) [123]. Enzymatic acceleration of this step is spectacular, approaching 12 orders of magnitude in the case of MMCM and GM [74,124,125], which corresponds to a reduction in the Co—C(Ado) bond dissociation enthalpy of AdoCbl from 131 kJ/mol in the free cofactor to ~59 kJ/mol in the enzyme-bound form. The Ado• radical generated in this process then abstracts a hydrogen atom from substrate to initiate the protein-mediated carbon skeleton rearrangement. Reabstraction of the H atom from the adenosine moiety by the product radical and subsequent reformation of the cofactor's Co—C(Ado) bond complete the catalytic cycle [126].

The mechanism by which AdoCbl-dependent isomerases achieve their remarkable acceleration of Co—C(Ado) bond homolysis, without increasing the likelihood of potentially harmful side reactions, remains one of the greatest subjects of debate among B_{12} researchers. Viable strategies employed by these enzymes to lower the energetic barrier associated with the homolytic cleavage of the Co—C(Ado) bond include (i) destabilization of the AdoCbl "ground" state by the active site and/or subsequent binding of substrate to the holoenzyme, (ii) a stabilization of the $Co^{2+}Cbl$ and Ado• post-homolysis products (note that because Co—C bond homolysis is an endergonic process, the transition state should closely resemble the final state of this reaction), and (iii) a combination of (i) and (ii). MMCM and GM have been the subjects of a large number of spectroscopic studies [25,77,78,126–138] as well as purely theoretical investigations [139–143] to assess the feasibility of these strategies for enzymatic Co—C(Ado) bond activation.

To investigate how AdoCbl-dependent isomerases enhance the rate of Co—C(Ado) bond homolysis, our laboratory employed a combined spectroscopic/computational approach to probe the cofactor/active site interactions in both the AdoCbl "ground" state and the $Co^{2+}Cbl$ post-homolysis state. Abs and MCD spectra of MMCM reconstituted with the native cofactor AdoCbl were strikingly similar to those obtained for the unbound cofactors. This finding indicated that replacement of the axially coordinated DMB

by a His residue from the enzyme active site has insignificant effects on the electronic properties of the cofactors and provided compelling evidence that the long Co—N(His) bond observed by X-ray crystallography was presumably an artifact. Likewise, only minor perturbations to the Abs and MCD spectra were observed upon substrate (analogue) binding to holo-MMCM, thus arguing against models invoking substrate-induced enzymatic Co—C(Ado) bond activation.

Interestingly, somewhat more significant Abs and MCD spectral changes were noted upon substrate (analogue) binding to MMCM reconstituted with MeCbl, a sterically less constrained derivative of AdoCbl. To interpret these changes in terms of geometric perturbations of the cofactor, two sets of constrained DFT geometry optimizations were performed on MeCbl models in which either the Co—C(Me) bond or the axial Co—N bond were systematically elongated from their equilibrium positions. TDDFT computations were then performed on these perturbed MeCbl models to explore the effects of axial distortions along the Co—C(Me) and Co—N coordinates on the electronic transition energies and Abs intensities. These computations revealed that the α-band position provides an extremely sensitive reporter of changes in both the Co—C(Me) and Co—N bond lengths and permitted us to interpret the small red-shift of the α-band observed upon MeCbl binding to MMCM in terms of a minor Co—N bond decrease by 0.03 Å. Similarly, the small blue-shift of the α-band that was observed in response to substrate binding to the MMCM/MeCbl complex could be explained by an elongation of the lower axial Co—N bond by ∼0.08 Å. As no such changes were observed when the same set of experiments was performed with the native cofactor, we concluded that enzymatic perturbation of the AdoCbl cofactor in its Co^{3+}Cbl "ground" state produces an insignificant contribution to the dramatic acceleration of Co—C(Ado) bond homolysis by MMCM.

To explore whether enzymatic Co—C bond activation instead involves stabilization of the Co^{2+}Cbl post-homolysis product, we also performed a combined spectroscopic and DFT computational study of MMCM with the cofactor in the Co^{2+}Cbl state [78]. In contrast to the minor spectral perturbations accompanying AdoCbl-binding to MMCM, rather significant changes were noted between the MCD spectra of free and MMCM-bound Co^{2+}Cbl, especially in the presence of the "slow" substrate glutaryl-CoA (Fig. 13, bottom). To interpret these spectral differences in terms of changes in the cofactor's electronic structure, DFT and TDDFT calculations were carried out on a suitably truncated model of Co^{2+}Cbl to identify the specific donor and acceptor MOs involved in the relevant electronic transitions. The key results obtained in these computations are summarized in Fig. 13 (top). Building upon these computationally assisted spectral assignments for Co^{2+}Cbl, we were able to determine from our MCD data that binding of Co^{2+}Cbl to the MMCM active site, both in the absence and the presence of substrate, primarily affects the energies of the metal-to-ligand charge transfer (MLCT) transitions while leaving those of the LF and corrin-centered $\pi \rightarrow \pi^*$ transitions largely unchanged. To rationalize these findings, we invoked a roughly uniform stabilization of the Co 3d-based MOs relative to the corrin π/π^*-based orbitals. Importantly, because the former MOs are (partially) filled, lowering their energies should stabilize the enzyme-bound cofactor as a whole and thus produce a significant contribution to the enzymatic acceleration of Co—C(Ado) bond homolysis. The fact that the band shifts, and thus the stabilization of the MMCM-bound Co^{2+}Cbl species, are greatest when substrate is present in the active site led to the proposal that this enzyme has evolved so as to prevent formation of the Co^{2+}Cbl/Ado• radical pair in the absence of substrate, thereby protecting itself from deleterious side reactions that could otherwise occur.

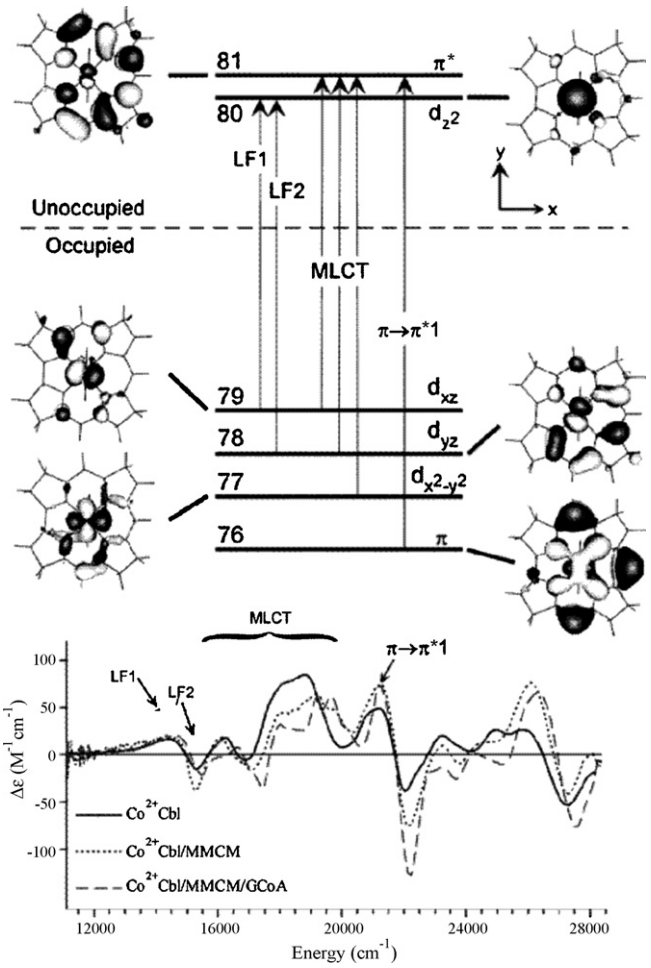

Fig. 13. Top: Relative energies and isosurface plots of the relevant spin-down MOs for Co^{2+}Cbl based on a spin-unrestricted DFT calculation. Electronic transitions that have been correlated to bands in the experimental Co^{2+}Cbl MCD spectrum (bottom) are indicated by vertical arrows. Bottom: 4.5 K MCD spectra of free Co^{2+}Cbl, MMCM-bound Co^{2+}Cbl (Co^{2+}Cbl/MMCM), and MMCM-bound Co^{2+}Cbl in the presence of the "slow" substrate glutaryl-CoA (Co^{2+}Cbl/MMCM/GCoA). Adapted from Ref. [78].

Building upon the insights gained in our research on MMCM, we subsequently performed a combined spectroscopic and DFT computational study of GM to explore whether these two isomerases employ the same basic strategy for Co—C(Ado) bond activation [127]. Analogous to the results obtained for MMCM, the Abs and MCD spectra of free and GM-bound AdoCbl were found to be virtually superimposable, indicating that in the latter enzyme the DMB → His axial ligand switch accompanying cofactor binding to the active site also has a minimal effect on the cofactor's Co—C bond. Additionally, the major differences in the MCD spectra of free and GM-bound Co^{2+}Cbl involved a uniform blue-shift of features attributed to MLCT transitions, just as we observed for MMCM. On the basis of this close resemblance between the spectroscopic data obtained for GM and MMCM, we proposed that these enzymes, and presumably also other AdoCbl-dependent isomerases, share a common mechanism for Co—C bond activation.

Very recently, two research groups have employed QM/MM computations to explore how the GM and MMCM active sites modulate the Co—C(Ado) bond homolysis rate. In one study, Ryde and co-workers have used this method to compute the potential energy associated with a distortion of the Co—C(Ado) bond of GM-bound AdoCbl from its equilibrium distance to the Co^{2+}Cbl/Ado• radical pair product state [143]. These calculations confirmed

an earlier proposal, originally put forth by Dölker et al. on the basis of DFT/B3LYP computations [142], that the product (i.e., post-homolysis) state is stabilized by an electrostatic interaction between the Co^{2+} ion and two oxygen atoms from the Ado• radical. In addition, they suggested that an even larger contribution to the enzymatic activation of the Co—C(Ado) bond involves the differential stabilization of the Ado moiety in the AdoCbl "ground" state and the post-homolysis state.

As stipulated by our spectroscopic data, QM/MM calculations performed by Paneth and co-workers have revealed that MMCM employs the same basic strategy for Co—C(Ado) bond activation as the one outlined above for GM [144]. An important finding from this study was that in the transition state of the Co—C(Ado) bond homolysis reaction, the corrin ring is only minimally perturbed while the Ado moiety is significantly distorted from its conformation adopted in the AdoCbl "ground" state. Consequently, as more and more experimental and computational results become available, it becomes increasingly clear that the differential stabilization of the Ado moiety and stabilization of the Co^{2+}Cbl post-homolysis product make the primary contributions to the remarkable acceleration of Co—C(Ado) bond homolysis achieved by the AdoCbl-dependent isomerases. Other factors may also be important, however. For example, a recent DFT computational study by Kozlowski et al. [145] revealed that the initial cleavage of the Co—C bond and subsequent H-atom abstraction from substrate may in fact occur in a concerted fashion, thereby leading to a significant stabilization of the transition state.

3.3. MeCbl-dependent methyltransferases

Cbl-dependent methyltransferases utilize the MeCbl and Co^{1+}Cbl forms of the B_{12} cofactor in order to catalyze the transfer of a methyl group between two substrates [79]. Though this family of enzymes includes several members with highly diverse functions, MetH is the only Cbl-dependent methyltransferase known to occur in humans. Because this enzyme shares high homology with the MetH from *Escherichia coli*, the latter represents one of the most extensively studied methyltransferases to date [146–148]. MetH catalyzes a methyl transfer from CH_3-THF to Hcy, thereby producing Met along with THF [46,47]. Consequently, this enzyme plays a vital role in maintaining a healthy distribution of cellular folate derivatives and preventing the accumulation of Hcy, a metabolite that is toxic in high concentrations [46,96,97]. MetH accelerates the rate of methyl transfer from MeCbl to Hcy by 10^6-fold relative to the non-enzymatic reaction in solution [149,150]. Seminal experimental studies by Matthews and co-workers revealed that this 10^6-fold rate enhancement can be divided into two separate contributions; namely, (i) a 10^2-fold enhancement associated with the binding of MeCbl to MetH and (ii) a 10^4-fold contribution stemming from Hcy binding to the enzyme [151]. Therefore, MetH must use a catalytic strategy that includes activation of both the cofactor and the substrate.

Jensen and Ryde performed DFT/B3LYP computations to locate and characterize the transition state associated with the MetH-catalyzed methyl transfer from MeCbl to Hcy [152]. Two potential strategies available to MetH to enhance the methyl transfer rate were then evaluated by calculating the transition-state energy under several reaction conditions (Fig. 14). The first strategy considered Hcy deprotonation by an enzyme-bound Zn^{2+} ion [153,154]. The DFT-computed activation energy for the methylation of neutral Hcy was 22 kcal/mol larger than that for the corresponding thiolate species, indicating that methyl transfer from MeCbl to neutral Hcy has a prohibitively large activation barrier. The second strategy investigated by DFT computations involved the creation of a hydrophobic environment for the reactants, as suggested by an analysis of the X-ray crystal structure of the Hcy binding module of MetH [155]. The results obtained in these calculations indicated that the lower dielectric constant associated with a hydrophobic active site can indeed drastically increase the rate of this reaction, by up to 10^{14}-fold. On the basis of these DFT computations, it was suggested that the 10^6-fold rate enhancement by MetH for the methyl transfer from MeCbl to Hcy is likely achieved via a combination of Hcy deprotonation by an enzyme-bound Zn^{2+} ion and the creation of a hydrophobic active site environment for the reactants.

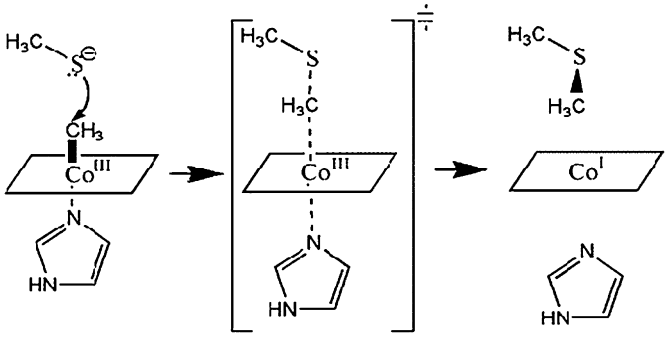

Fig. 14. The truncated model used in a DFT computational study of the methyl transfer reaction catalyzed by MetH. Adapted from Ref. [152].

In support of this proposal, a combined spectroscopic and DFT computational study confirmed that in the MetH conformation relevant to methyl transfer, the active site bound cofactor is in a hydrophobic environment [80]. Specifically, by mutating the His759 residue that coordinates axially to the MeCbl cofactor under turnover conditions to a Gly, we were able to trap and characterize MetH locked into a catalytic conformation with the cofactor in the Co^{2+}Cbl state. The MCD spectrum of this species was found to exhibit an intense, positively signed band at a significantly lower energy than any feature observed in the free Co^{2+}Cbl and Co^{2+}Cbi$^+$ MCD spectra [27]. Instead, this spectrum closely resembled the MCD spectra of the "activated" Co^{2+}corrinoid species bound to the ATR active sites (Fig. 7), as discussed in Section 3.1. Likewise, a fit of the EPR spectrum of this H759G MetH-bound Co^{2+}Cbl species yielded g values and $A(^{59}Co)$ hyperfine coupling constants that are significantly larger than those reported for Co^{2+}Cbl and Co^{2+}Cbi$^+$ but similar to those obtained for the ATR-bound Co^{2+}corrinoid species. Consequently, we were able to analyze the MCD and EPR spectroscopic data of the H759G MetH-bound Co^{2+}Cbl species by using the spectro/structural correlations we developed for Co^{2+}Cbi$^+$ (*vide supra*) [110]. This analysis revealed that the enzyme induces (partial) dissociation of the cofactor's axial ligand to generate an effectively four-coordinate Co^{2+}Cbl species without any significant axial bonding interactions. Since four-coordinate Co^{2+}Cbl and Co^{2+}Cbi$^+$ are energetically unstable in aqueous solution [108], this result indicated that solvent must be excluded from the MetH active site in the enzyme conformations relevant to methyl transfer. As discussed above [152], the creation of this hydrophobic active site environment should make a significant contribution to the enzymatic acceleration of methyl transfer from MeCbl to Hcy [149,150].

A second Cbl-dependent methyltransferase that has been studied by DFT is the corrinoid/iron-sulfur protein (CFeSP) from *Moorella thermoacetica* [156–158]. The physiological role of CFeSP is to shuttle a methyl group from the CH_3-THF:CFeSP methyltransferase to one of the two Ni centers of the active site A-cluster of acetyl-coenzyme A synthase (ACS) [159–162]. Ragsdale and coworkers determined that CFeSP increases the rate of methyl transfer from MeCbl to ACS by 10^5-fold, or 10^2-fold relative to the rate for methyl transfer from free MeCbi$^+$ [163].

A combined spectroscopic and DFT study of CFeSP led to the suggestion that the strategy employed by this enzyme to achieve the 10^5-fold rate enhancement for the methyl transfer from MeCbl to the ACS A-cluster may be fundamentally different from that used by MetH [164]. While in MetH the MeCbl cofactor is axially coordinated by a protein-derived His residue (H759, *vide supra*), CFeSP binds MeCbl in the "base-off" form with a solvent-derived water molecule completing a six-coordinate Co^{3+} ligand environment, as in aqueous $MeCbi^+$. Based on a comparison of the rates for methyl transfer from free MeCbl and $MeCbi^+$ to ACS, substitution of an axially bound nitrogen donor by a more weakly σ-donating oxygen donor should only cause an $\sim 10^3$-fold rate enhancement by the enzyme [163]. Yet, detailed Abs and MCD spectroscopic studies revealed that CFeSP-bound MeCbl and free $MeCbi^+$ actually possess somewhat different electronic structures, as evidenced by the fact that the α-band of the enzyme-bound species is blue-shifted (by 390 cm^{-1}) from that of free $MeCbi^+$. By developing a spectro/structural correlation for $MeCbi^+$ using DFT/B3LYP computations, we were able to correlate this blue-shift to an elongation of the Co—OH_2 bond by about 0.2 Å in the CFeSP-bound MeCbl species [26]. This elongation of the Co—OH_2 bond from ~2.20 to 2.40 Å was proposed to make the cobalt center more "Co^{1+}-like", thereby facilitating heterolytic Co—C bond cleavage. In support of this proposal, a recent DFT/B3LYP computational study revealed that elongation of the α-axial ligand–Co bond should favor Co—C bond heterolysis by destabilizing the MeCbl state relative to the Co^{1+}Cbl state [56]. Therefore, the 10^5-fold rate enhancement by CFeSP for the methyl transfer from MeCbl to the ACS A-cluster presumably stems from the α-axial ligand switch and Co—OH_2 bond elongation.

Occasionally, the Co^{1+}Cbl intermediate that is generated in the MetH and CFeSP active sites by methyl transfer from MeCbl to substrate is accidentally oxidized to the inactive Co^{2+}Cbl form [81,165], which must be reactivated in a process that requires the enzymes to catalyze the thermodynamically challenging $Co^{2+} \rightarrow Co^{1+}$ reduction [98]. While the CFeSP protein additionally hosts a low-potential $[Fe_4S_4]^{2+/1+}$ cluster ($E^\circ = -523$ mV vs. SHE) [166] that can readily reduce the "base-off" Co^{2+}Cbl species bound to the enzyme active site ($E^\circ \approx -490$ mV, based on the reduction potential of free $Co^{2+}Cbi^+$) [167], this process represents a significant challenge for MetH, which utilizes an external electron donor, such as flavodoxin ($E^\circ = -440$ mV) [98], to reduce the inactive Co^{2+}Cbl form.

To explore how MetH overcomes this challenge, we prepared and characterized the Co^{2+}Cbl-bound state of the H759G variant of MetH locked into the activation conformation [80], as opposed to a catalytic conformation as we did to assess the hydrophobicity of the MetH active site (*vide supra*). The MCD and EPR spectra obtained for this species were found to be very similar to those of free $Co^{2+}Cbi^+$ [27], which we interpreted to indicate that MetH possesses a five-coordinate Co^{2+}Cbl species with an axially coordinated water molecule in the activation conformation. However, the MeCbl-bound form of this MetH variant, which was prepared via reductive methylation of the corresponding Co^{2+}Cbl containing species, exhibited Abs and MCD spectra that were strikingly different from the spectra of either free MeCbl or $MeCbi^+$ [26]. Most importantly, the α-band of the enzyme-bound MeCbl species occurred at a significantly higher energy than those of any alkyl-Co^{3+}Cbl species investigated, including the CFeSP-bound MeCbl species described above [164]. On the basis of the spectro/structural correlations established for $MeCbi^+$, the magnitude of this blue-shift observed for H759G MetH-bound MeCbl could be correlated with an axial Co—OH_2 bond elongation by at least 0.9 Å. This result suggested that a five-coordinate form of MeCbl is most likely formed in the active site when MetH is in the activation conformation. Since a five-coordinate Co^{3+}Cbl species is unstable in aqueous solution [108], this result indicated that solvent was excluded from the α-face of the cofactor during Co^{2+}Cbl activation by MetH. Consequently, the water molecule that was found to be axially coordinated in the Co^{2+}Cbl-bound form of this variant must be located on the β-face and thus in an ideal position to be removed by the nearby Y1139 residue upon binding of *S*-adenosylmethionine to the enzyme active site, so as to ensure rapid $Co^{2+} \rightarrow Co^{1+}$ reduction during reductive methylation of the cofactor [168].

4. Conclusions

Collectively, the dedicated efforts of enzymologists, spectroscopists, and X-ray crystallographers have established an excellent foundation for the successful completion of computational studies aimed at elucidating the electronic structures of the B_{12} cofactors and the catalytic cycles of enzymes that utilize these unusual bio-organometallic species to carry out chemically challenging substrate-rearrangement and methyl transfer reactions. As described in Section 2, the results provided by experimentally validated DFT computations have not only drastically enhanced our understanding of the relationships that exist between the geometric, electronic, and spectral properties of the B_{12} cofactors in their Co^{3+}, Co^{2+}, and Co^{1+} oxidation states, but they also established an excellent framework to interpret spectral changes accompanying the binding of these species to enzyme active sites in terms of perturbations to their geometric and electronic structures. Computational studies have also played a vital role in elucidating key steps in the Co—C(Ado) bond-formation process catalyzed by ATRs as well as the catalytic cycles of AdoCbl-dependent enzymes. In the case of the ATRs, computationally assisted analyses of spectroscopic data revealed that these enzymes catalyze the thermodynamically challenging $Co^{2+} \rightarrow Co^{1+}$ reduction by generating an essentially square-planar Co^{2+}corrinoid intermediate, so as to stabilize the redox-active, Co $3d_{z^2}$-based molecular orbital that is pointing toward the axial coordination sites of the Co^{2+} ion. A common mechanism also appears to be utilized by AdoCbl-dependent enzymes for accelerating the rate of homolytic cleavage of the cofactor's Co—C(Ado) bond upon binding of substrate to the active site. Specifically, growing experimental and computational evidence suggests that these enzymes lower the activation barrier for Co—C(Ado) bond homolysis by preferentially stabilizing the Co^{2+}Cbl/ Ado$^\bullet$ radical pair (i.e., the product state). In contrast, because the MeCbl-dependent enzymes most likely use a catalytic strategy that involves activation of both the cofactor and the substrate, relatively little consensus has been reached regarding the mechanism of enzyme-catalyzed Co—C(Me) bond heterolysis.

Acknowledgements

T.C.B. thanks his current and former graduate students and postdoctoral fellows for their hard work and valuable discussions on this project, especially Dr. Troy Stich and Dr. Amanda Reig (formerly Brooks), his superb collaborators for generous protein supply, Prof. Frank Neese for a free copy of his ORCA computational software package and his advice on electronic structure calculations, Katherine M. Van Heuvelen for her careful reading of this manuscript, and acknowledges the National Science Foundation (CAREER award MCB-0238530) for financial support.

References

[1] E.L. Rickes, N.G. Brink, F.R. Koniuszy, T.R. Wood, K. Folkers, Science 107 (1948) 396.

[2] D.C. Hodgkin, J. Pickworth, J.H. Robertson, K.N. Trueblood, R.J. Prosen, J.G. White, Nature (Lond.) 176 (1955) 325.
[3] L. Ouyang, P. Rulis, W.Y. Ching, G. Nardin, L. Randaccio, Inorg. Chem. 43 (2004) 1235.
[4] B. Kraütler, W. Keller, C. Kratky, J. Am. Chem. Soc. 111 (1989) 8938.
[5] C.H. Martin, M.C. Zerner, in: E.I. Solomon, A.B.P. Lever (Eds.), Inorganic Electronic Structure and Spectroscopy, John Wiley & Sons, Inc., New York, NY, 1999, p. 555.
[6] F. Neese, T. Petrenko, D. Ganyushin, G. Olbrich, Coord. Chem. Rev. 251 (2007) 288.
[7] A. Ghosh, P.R. Taylor, Curr. Opin. Chem. Biol. 7 (2003) 113.
[8] B.O. Roos, U. Ryde, in: A.B.P. Lever (Ed.), Fundamentals: Physical Methods, Theoretical Analysis, and Case Studies, Elsevier Pergamon, Amsterdam, 2004, p. 457.
[9] F. Neese, J. Biol. Inorg. Chem. 11 (2006) 702.
[10] T. Lovell, F. Himo, W.-G. Han, L. Noodleman, Coord. Chem. Rev. 238–239 (2003) 211.
[11] L. Randaccio, S. Geremia, G. Nardin, J. Wuerges, Coord. Chem. Rev. 250 (2006) 1332.
[12] C.B. Perry, H.M. Marques, S. Afr. J. Sci. 100 (2004) 368.
[13] E. Mayer, D.J. Gardiner, R.E. Hester, Mol. Phys. 26 (1973) 783.
[14] E. Mayer, D.J. Gardiner, S.R. Harder, J. Chem. Soc., Faraday Trans. 2 (69) (1973) 1350.
[15] W.T. Wozniak, T.G. Spiro, J. Am. Chem. Soc. 95 (1973) 3402.
[16] W.O. George, R. Mendelsohn, Appl. Spectrosc. 27 (1973) 390.
[17] F. Galluzzi, M. Garozzo, F.F. Ricci, J. Raman Spectrosc. 2 (1974) 351.
[18] C.-W. Tsai, M.D. Morris, Anal. Chim. Acta 76 (1975) 193.
[19] S. Salama, T.G. Spiro, J. Raman Spectrosc. 6 (1977) 57.
[20] S. Nie, P.A. Marzilli, L.G. Marzilli, N.-T. Yu, J. Chem. Soc., Chem. Commun. (1990) 770.
[21] L. Quaroni, J. Reglinski, W.E. Smith, J. Raman Spectrosc. 26 (1995) 1075.
[22] J.M. Puckett, M.B. Mitchell, S. Hirota, L.G. Marzilli, Inorg. Chem. 35 (1996) 4656.
[23] S. Dong, R. Padmakumar, R.V. Banerjee, T.G. Spiro, J. Am. Chem. Soc. 118 (1996) 9182.
[24] S. Dong, R. Padmakumar, R.V. Banerjee, T.G. Spiro, Inorg. Chim. Acta 270 (1998) 392.
[25] S. Dong, R. Padmakumar, N. Maiti, R. Banerjee, T.G. Spiro, J. Am. Chem. Soc. 120 (1998) 9947.
[26] T.A. Stich, A.J. Brooks, N.R. Buan, T.C. Brunold, J. Am. Chem. Soc. 125 (2003) 5897.
[27] T.A. Stich, N.R. Buan, T.C. Brunold, J. Am. Chem. Soc. 126 (2004) 9735.
[28] M.D. Liptak, T.C. Brunold, J. Am. Chem. Soc. 128 (2006) 9144.
[29] S. Van Doorslaer, G. Jeschke, B. Epel, D. Goldfarb, R.-A. Eichel, B. Kraütler, A. Schweiger, J. Am. Chem. Soc. 125 (2003) 5915.
[30] J. Harmer, S. Van Doorslaer, I. Gromov, A. Schweiger, Chem. Phys. Lett. 358 (2002) 8.
[31] G.N. Schrauzer, L.-P. Lee, J. Am. Chem. Soc. 90 (1968) 6541.
[32] J.H. Bayston, F.D. Looney, J.R. Pilbrow, M.E. Winfield, Biochemistry 9 (1970) 2164.
[33] R. Banerjee, S. Chowdhury, in: R. Banerjee (Ed.), Chemistry and Biochemistry of B_{12}, John Wiley & Sons, Inc., New York, 1999, p. 707.
[34] M. Flavin, P.J. Ortiz, S. Ochoa, Nature (Lond.) 176 (1955) 823.
[35] J. Katz, I.L. Chaikoff, J. Am. Chem. Soc. 77 (1955).
[36] E.N.G. Marsh, Bioorg. Chem. 28 (2000) 176.
[37] P.A. Frey, Annu. Rev. Biochem. 70 (2001) 121.
[38] K. Gruber, C. Kratky, Curr. Opin. Chem. Biol. 6 (2002) 598.
[39] R. Banerjee, Chem. Rev. 103 (2003) 2083.
[40] T. Toraya, Chem. Rev. 103 (2003) 2095.
[41] C.M. Dobson, T. Wai, D. Leclerc, H. Kadir, M. Narang, J.P. Lerner-Ellis, T.J. Hudson, D.S. Rosenblatt, R.A. Gravel, Hum. Mol. Genet. 11 (2002) 3361.
[42] N.A. Leal, S.D. Park, P.E. Kima, T.A. Bobik, J. Biol. Chem. 278 (2003) 9227.
[43] C.B. Bauer, M.V. Fonseca, H.M. Holden, J.B. Thoden, T.B. Thompson, J.C. Escalante-Semerena, I. Rayment, Biochemistry 40 (2001) 361.
[44] C.L.V. Johnson, M.L. Buszko, T.A. Bobik, J. Bacteriol. 186 (2004) 7881.
[45] N.R. Buan, S.J. Suh, J.C. Escalante-Semerena, J. Bacteriol. 186 (2004) 5708.
[46] R.G. Matthews, in: R. Banerjee (Ed.), Chemistry and Biochemistry of B_{12}, John Wiley & Sons, Inc., New York, 1999, p. 681.
[47] R.T. Taylor, H. Weissbach, J. Biol. Chem. 242 (1967) 1502.
[48] S.W. Ragsdale, in: R. Banerjee (Ed.), Chemistry and Biochemistry of B_{12}, John Wiley & Sons, Inc., New York, 1999, p. 633.
[49] K. Sauer, R.K. Thauer, in: R. Banerjee (Ed.), Chemistry and Biochemistry of B_{12}, John Wiley & Sons, Inc., New York, 1999, p. 655.
[50] T. Andruniow, P.M. Kozlowski, M.Z. Zgierski, J. Chem. Phys. 115 (2001) 7522.
[51] T. Andruniow, J. Kuta, M.Z. Zgierski, P.M. Kozlowski, Chem. Phys. Lett. 410 (2005) 410.
[52] T. Andruniow, M.Z. Zgierski, P.M. Kozlowski, Chem. Phys. Lett. 331 (2000) 502.
[53] T. Andruniow, M.Z. Zgierski, P.M. Kozlowski, J. Phys. Chem. B 104 (2000) 10921.
[54] T. Andruniow, M.Z. Zgierski, P.M. Kozlowski, J. Am. Chem. Soc. 123 (2001) 2679.
[55] T. Andruniow, M.Z. Zgierski, P.M. Kozlowski, J. Phys. Chem. A 106 (2002) 1365.
[56] N. Dölker, F. Maseras, A. Lledos, J. Phys. Chem. B 107 (2003) 306.
[57] P.M. Kozlowski, T. Andruniow, A.A. Jarzecki, M.Z. Zgierski, T.G. Spiro, Inorg. Chem. 45 (2006) 5585.
[58] J. Kuta, S. Patchkovskii, M.Z. Zgierski, P.M. Kozlowski, J. Comput. Chem. 27 (2006) 1429.
[59] C. Rovira, X. Biarnes, K. Kunc, Inorg. Chem. 43 (2004) 6628.
[60] C. Rovira, K. Kunc, J. Hutter, M. Parrinello, Inorg. Chem. 40 (2001) 11.
[61] C. Rovira, P.M. Kozlowski, J. Phys. Chem. B 111 (2007) 3251.
[62] J.P. Bouquiere, J.L. Finney, M.S. Lehmann, P.F. Lindley, H.F. Savage, Acta Cryst. Sec. B: Struct. Commun. 49 (1993) 79.
[63] C. Kratky, G. Farber, K. Gruber, K. Wilson, Z. Dauter, H.-F. Nolting, R. Konrat, B. Kraütler, J. Am. Chem. Soc. 117 (1995) 4654.
[64] L. Randaccio, M. Furlan, S. Geremia, M. Slouf, I. Srnova, D. Toffoli, Inorg. Chem. 39 (2000) 3403.
[65] C. Lee, W. Yang, R.G. Parr, Phys. Rev. B: Condens. Matter 37 (1988) 785.
[66] A.D. Becke, Phys. Rev. A 38 (1988) 3098.
[67] A.D. Becke, J. Chem. Phys. 98 (1993) 5648.
[68] R.A. Firth, H.A.O. Hill, J.M. Pratt, R.J.P. Williams, W.R. Jackson, Biochemistry 6 (1967) 2178.
[69] J.M. Pratt, in: R. Banerjee (Ed.), Chemistry and Biochemistry of B_{12}, Wiley, New York, 1999, p. 113.
[70] J.I. Toohey, Proc. Natl. Acad. Sci. U.S.A. 54 (1965) 934.
[71] M.V. Fonseca, J.C. Escalante-Semerena, J. Bacteriol. 182 (2000) 4304.
[72] R. Banerjee, Chemistry and Biochemistry of B_{12}, John Wiley & Sons, Inc., New York, 1999.
[73] R. Banerjee, Biochemistry 40 (2001) 6191.
[74] S. Chowdhury, R. Banerjee, Biochemistry 39 (2000) 7998.
[75] E.N.G. Marsh, D.P. Ballou, Biochemistry 37 (1998) 11864.
[76] K.L. Brown, X. Zou, J. Inorg. Biochem. 77 (1999) 185.
[77] A.J. Brooks, M. Vlasie, R.V. Banerjee, T.C. Brunold, J. Am. Chem. Soc. 126 (2004) 8167.
[78] A.J. Brooks, M. Vlasie, R. Banerjee, T.C. Brunold, J. Am. Chem. Soc. 127 (2005) 16522.
[79] R.G. Matthews, Acc. Chem. Res. 34 (2001) 681.
[80] M.D. Liptak, A.S. Fleishchhacker, R.G. Matthews, T.C. Brunold, Biochemistry 46 (2007) 8024.
[81] J.T. Drummond, S. Huang, R.M. Blumenthal, R.G. Matthews, Biochemistry 32 (1993) 9290.
[82] K. Fujii, F.M. Huennekens, J. Biol. Chem. 249 (1974) 6745.
[83] J.H. Mangum, K.G. Scrimgeour, Fed. Proc. 21 (1962) 242.
[84] J.C. Escalante-Semerena, S.-J. Suh, J.R. Roth, J. Bacteriol. 172 (1990) 273.
[85] M.R. Rondon, J.R. Trzebiatowski, J.C. Escalante-Semerena, Prog. Nucleic Acid Res. Mol. Biol. 56 (1997) 347.
[86] M.V. Fonseca, J.C. Escalante-Semerena, J. Biol. Chem. 276 (2001) 32101.
[87] F. Neese, J. Chem. Phys. 115 (2001) 11080.
[88] S.H. Vosko, L. Wilk, M. Nusair, Can. J. Phys. 58 (1980) 1200.
[89] J.P. Perdew, Phys. Rev. B: Condens. Matter 33 (1986) 8822.
[90] A.D. Becke, J. Chem. Phys. 98 (1993) 1372.
[91] J.P. Perdew, Y. Wang, Phys. Rev. B: Condens. Matter 45 (1992) 13244.
[92] M.K. Johnson, in: J. Lawrence Que (Ed.), Physical Methods in Bioinorganic Chemistry, University Science Books, Sausalito, CA, 2000, p. 233.
[93] R.V. Banerjee, V. Frasca, D.P. Ballou, R.G. Matthews, Biochemistry 29 (1990) 11101.
[94] N.A. Leal, H. Olteanu, R. Banerjee, T.A. Bobik, J. Biol. Chem. 279 (2004) 47536.
[95] C. Holliger, G. Wohlfarth, G. Diekert, FEMS Microbiol. Rev. 22 (1999) 383.
[96] S.P. Stabler, R.H. Allen, Annu. Rev. Nutr. 24 (2004) 299.
[97] R.V. Banerjee, R.G. Matthews, FASEB J. 4 (1990) 1450.
[98] J.T. Jarrett, D.M. Hoover, M.L. Ludwig, R.G. Matthews, Biochemistry 37 (1998) 12649.
[99] K.P. Jensen, U. Ryde, ChemBioChem 4 (2003) 413.
[100] D.A. Pratt, W.A. van der Donk, J. Am. Chem. Soc. 127 (2005) 384.
[101] M. Jaworska, P. Lodowski, Theochem 631 (2003) 209.
[102] M. Giorgetti, I. Ascone, M. Berrettoni, P. Conti, S. Zamponi, R. Marassi, J. Biol. Inorg. Chem. 5 (2000) 156.
[103] M.D. Wirt, I. Sagi, M.R. Chance, Biophys. J. 63 (1992) 412.
[104] J.M. Pratt, Inorganic Chemistry of Vitamin B_{12}, Academic Press Inc., New York, 1972.
[105] J.P. Perdew, K. Burke, M. Ernzerhof, Phys. Rev. Lett. 77 (1996) 3865.
[106] E.M. Sampson, C.L.V. Johnson, T.A. Bobik, Microbiology 151 (2005) 1169.
[107] H. Olteanu, K.R. Wolthers, A.W. Munro, N.S. Scrutton, R. Banerjee, Biochemistry 43 (2004) 1988.
[108] D. Lexa, J.M. Saveant, Acc. Chem. Res. 16 (1983) 235.
[109] L. Mciver, C. Leadbeater, D.J. Campopiano, R.L. Baxter, S.N. Daff, S.K. Chapman, A.W. Munro, Eur. J. Biochem. 257 (1998) 557.
[110] T.A. Stich, N.R. Buan, J.C. Escalante-Semerena, T.C. Brunold, J. Am. Chem. Soc. 127 (2005) 8710.
[111] T.A. Stich, M. Yamanishi, R. Banerjee, T.C. Brunold, J. Am. Chem. Soc. 127 (2005) 7660.
[112] K. Park, P.E. Mera, J.C. Escalante-Semerena, T.C. Brunold, Biochemistry 47 (2008) 9007.
[113] D.J. Szalda, C.L. Schwarz, J.F. Endicott, E. Fujita, C. Creutz, Inorg. Chem. 28 (1989) 3214.
[114] V.L. Goedken, N.K. Kjeldahl, D.H. Busch, J. Coord. Chem. 7 (1977) 89.
[115] G. Palmer, in: L. Que Jr. (Ed.), Physical Methods in Bioinorganic Chemistry, University Science Books, Sausalito, CA, 2000, p. 121.
[116] R. Banerjee, Chem. Biol. 4 (1997) 175.
[117] R. Banerjee, S.W. Ragsdale, Annu. Rev. Biochem. 72 (2003) 209.
[118] S.M. Matsui, M.J. Mahoney, L.E. Rosenberg, N. Engl. J. Med. 308 (1983) 857.
[119] F. Mancia, N.H. Keep, A. Nakagawa, P.F. Leadlay, S. McSweeney, B. Rasmussen, P. Bosecke, O. Diat, P.R. Evans, Structure 4 (1996) 339.

[120] R. Jansen, F. Kalousek, W.A. Fenton, L.E. Rosenberg, F.D. Ledley, Genomics 4 (1989) 198.
[121] H.A. Barker, V. Rooze, F. Suzuki, A.A. Iodice, J. Biol. Chem. 239 (1964) 3260.
[122] K. Gruber, R. Reitzer, C. Kratky, Angew. Chem. (Int. Ed.) 40 (2001) 3377.
[123] N.H. Thoma, T.W. Meier, P.R. Evans, P.F. Leadlay, Biochemistry 39 (1998) 14386.
[124] B.P. Hay, R.G. Finke, J. Am. Chem. Soc. 108 (1986) 4820.
[125] B.P. Hay, R.G. Finke, J. Am. Chem. Soc. 109 (1987) 8012.
[126] S. Dong, R. Padmakumar, R. Banerjee, T.G. Spiro, J. Am. Chem. Soc. 121 (1999) 7063.
[127] A.J. Brooks, C.C. Fox, E.N.G. Marsh, M. Vlasie, R. Banerjee, T.C. Brunold, Biochemistry 44 (2005) 15167.
[128] R. Padmakumar, R. Banerjee, J. Biol. Chem. 270 (1995) 9295.
[129] D. Padovani, R. Banerjee, Biochemistry 45 (2006) 2951.
[130] R. Padmakumar, S. Taoka, R. Padmakumar, R. Banerjee, J. Am. Chem. Soc. 117 (1995) 7033.
[131] S. Chowdhury, R. Banerjee, Biochemistry 38 (1999) 15287.
[132] M. Vlasie, S. Chowdhury, R. Banerjee, J. Biol. Chem. 277 (2002) 18523.
[133] N.H. Thoma, P.R. Evans, P.F. Leadlay, Biochemistry 39 (2000) 9213.
[134] L. Xia, D.P. Ballou, E.N.G. Marsh, Biochemistry 43 (2004) 3238.
[135] P. Madhavapeddi, D.P. Ballou, E.N.G. Marsh, Biochemistry 41 (2002) 15803.
[136] H.-P. Chen, E.N.G. Marsh, Biochemistry 36 (1997) 7884.
[137] M. Yoon, A. Patwardhan, C. Qiao, S.O. Mansoorabadi, A.L. Menefee, G.H. Reed, E.N.G. Marsh, Biochemistry (2006).
[138] M.S. Huhta, H.-P. Chen, C. Hemann, C.R. Hille, E.N.G. Marsh, Biochem. J. 355 (2001) 131.
[139] S.D. Wetmore, D.M. Smith, B.T. Golding, L. Radom, J. Am. Chem. Soc. 123 (2001) 7963.
[140] D.M. Smith, B.T. Golding, L. Radom, J. Am. Chem. Soc. 121 (1999) 1383.
[141] D.M. Smith, B.T. Golding, L. Radom, J. Am. Chem. Soc. 121 (1999) 9388.
[142] N. Dölker, F. Maseras, P.E.M. Siegbahn, Chem. Phys. Lett. 386 (2004) 174.
[143] K.P. Jensen, U. Ryde, J. Am. Chem. Soc. 127 (2005) 9117.
[144] R.A. Kwiecien, I.V. Khavrutskii, D.G. Musaev, K. Morokuma, R. Banerjee, P. Paneth, J. Am. Chem. Soc. 128 (2006) 1287.
[145] P.M. Kozlowski, T. Kamachi, T. Toraya, K. Yoshizawa, Angew. Chem. (Int. Ed.) 46 (2007) 980.
[146] Y.N. Li, S. Gulati, P.J. Baker, L.C. Brody, R. Banerjee, W.D. Kruger, Hum. Mol. Genet. 5 (1996) 1851.
[147] D. Leclerc, E. Campeau, P. Goyette, C.E. Adjalla, B. Christensen, M. Ross, P. Eydoux, D.S. Rosenblatt, R. Rozen, R.A. Gravel, Hum. Mol. Genet. 5 (1996) 1867.
[148] L.H. Chen, M.-L. Liu, H.-Y. Hwang, L.-S. Chen, J. Korenberg, B. Shane, J. Biol. Chem. 272 (1997) 3628.
[149] H.P.C. Hogenkamp, G.T. Bratt, S.-Z. Sun, Biochemistry 24 (1985) 6428.
[150] V. Bandarian, R.G. Matthews, Biochemistry 40 (2001) 5056.
[151] C.W. Goulding, D. Postigo, R.G. Matthews, Biochemistry 36 (1997) 8082.
[152] K.P. Jensen, U. Ryde, J. Am. Chem. Soc. 125 (2003) 13970.
[153] J.T. Jarrett, C.Y. Choi, R.G. Matthews, Biochemistry 36 (1997) 15739.
[154] C.W. Goulding, R.G. Matthews, Biochemistry 36 (1997) 15749.
[155] J.C. Evans, D.P. Huddler, M.T. Hilgers, G. Romanchuk, R.G. Matthews, M.L. Ludwig, Proc. Natl. Acad. Sci. U.S.A. 101 (2004) 3729.
[156] L.G. Ljungdahl, J. LeGall, J.-P. Lee, Biochemistry 12 (1973) 1802.
[157] W.-P. Lu, I. Schiau, J.R. Cunningham, S.W. Ragsdale, J. Biol. Chem. 268 (1993) 5605.
[158] T. Svetlitchnaia, V. Svetlitchnyi, O. Meyer, H. Dobbek, Proc. Natl. Acad. Sci. U.S.A. 103 (2006) 14331.
[159] T. Doukov, J. Seravalli, J.J. Stezowski, S.W. Ragsdale, Structure 8 (2000) 817.
[160] T. Doukov, H. Hemmi, C.L. Drennan, S.W. Ragsdale, J. Biol. Chem. 282 (2007) 6609.
[161] W.-P. Lu, S.R. Harder, S.W. Ragsdale, J. Biol. Chem. 265 (1990) 3124.
[162] X.S. Tan, C. Sewell, P.A. Lindahl, J. Am. Chem. Soc. 124 (2002) 6277.
[163] J. Seravalli, K.L. Brown, S.W. Ragsdale, J. Am. Chem. Soc. 123 (2001) 1786.
[164] T.A. Stich, J. Seravalli, S. Venkateshrao, T.G. Spiro, S.W. Ragsdale, T.C. Brunold, J. Am. Chem. Soc. 128 (2006) 5010.
[165] S. Menon, S.W. Ragsdale, J. Biol. Chem. 274 (1999) 11513.
[166] S.R. Harder, W.-P. Lu, B.A. Feinberg, S.W. Ragsdale, Biochemistry 28 (1989) 9080.
[167] D. Lexa, J.M. Saveant, J. Zickler, J. Am. Chem. Soc. 102 (1980) 4851.
[168] M.D. Liptak, S. Datta, R.G. Matthews, T.C. Brunold, J. Am. Chem. Soc., 130 (in press).
[169] S.V. Doorslaer, G. Jeschke, B. Epel, D. Goldfarb, R.-A. Eichel, B. Käutler, A. Schweiger, J. Am. Chem. Soc. 125 (2003) 5915.
[170] F. Neese, University of Konstanz, 1997.